MEMO
Fokker Space & Systems B.V.
P.O.Box 32070
2303 DB Leiden
The Netherlands

SAX

document FSS-MG-R95-015
issue 1
date 21 Apr 1995
page i

security class	order no.	work package no.
Restricted		

title

SAX closed loop control in the gyro-less mode

summary

This document discusses the closed-loop control problems which are specific to the gyro-less mode of the SAX satellite. These problems include :

- excessive sensor quantization effects.
- kinematic and inertial cross-coupling during slews.
- attitude observability problems during eclipse.

The problems are discussed, and tuning methods and suggested parameter values are given for adapted gains of the PD control law and adapted structures and gains of the reconstructor filter. All solutions proposed fit in the framework of the current on-board software without code modifications.

	name	department	date	signature
prepared	P. Lammertse	FSS/PS	21 Apr 1995	
approved	F. v.d. Laan	FSS/PS		

Contents

Distribution List

controlled copies		uncontrolled copies
L. Karsten	FSS/EN	
J. Kouwen	FSS/R	
F. v.d. Laan	FSS/PS	
P. Lammertse	FSS/PS	
J. van Schie	SAX archive	

Revision Record

issue/ rev.	date	pages affected	brief description of change
1	25 Apr 1995	all	new document

1 Introduction

1.1 Control problems in the gyro-less mode

Two potential control problems have been identified in the gyro-less mode proposed for the SAX satellite. These are :

- excessive sensor quantization effects.
- kinematic and inertial cross-coupling in large slews.
- attitude observability problems during eclipse.

This note will discuss details and proposed solutions to these problems. This introductory chapter first gives an outline of the current control philosophy in SAX. It then proceeds to discuss in general terms the problems just mentioned, and selects some possible strategies for solving them. Later chapters discuss some of these strategies in more detail.

The attitude observability problem during eclipse is touched upon only briefly in this note, since it is an issue which goes somewhat beyond the scope of the closed-loop control problem proper.

1.2 Elements of the closed loop control

The closed loop control algorithms for SAX follow the approach of combining an augmented state reconstructor with a PD control law. Integrating control is implicit in the 'augmented' or extra states which model the long-term 'external' disturbances, viz. the 'external' disturbance torque and the gyro drift. An extra low-pass filter was added in SAX, in the loop between sensor output and estimator.

The 'separation principle' holds for linear systems. It states that the estimator performance and the feedback controller performance are independent. The feedback controller does not control the satellite attitude proper, but rather the estimated state of the satellite, a model of reality. The accuracy of the attitude estimate on the other hand is independent of the actions of the feedback controller (since those actions are supposedly known exactly to the estimator). The total inaccuracy of the attitude with respect to the target is the sum of the inaccuracy in the attitude estimate, and the inaccuracy in the station keeping performance of the control law.

1.3 Comparison to PID integrating control

An alternative to the augmented state observer - PD law combination is using straight noise filtering and PID control. This approach is in many ways similar to the observer - PD law combination. The difference is that it does not make use of two pieces of information which are used by the state estimator :

- a priori knowledge on the structure of the system (i.e. a 'model' of the actual system).
- knowledge of the torque commands that the controller itself has issued over the previous time steps.

This information allows the estimator to discriminate between attitude offsets which are caused by initial conditions (such as are due to setpoint updates at the start of a slew), and attitude offsets which are due to external influences, e.g. from disturbance torques. An integrating controller generally has to be stopped or reset during slews after a setpoint update, to prevent the perfectly legal attitude error from winding up the integrator. A disturbance torque estimator on the other hand can be left active at all times. Due to this extra use of information, both the step reponse and the stochastic performance of an estimator are superior to those of a straight PID controller.

The advantage of a state reconstructor breaks down as soon as the extra information is inaccurate enough to spoil the advantage. This point is reached fairly quickly : most state reconstructors do not take kindly to modelling errors or unmodelled disturbances. The state reconstructor approach is, in that sense, less robust to mistakes and oversights in the design phase than conventional PID control.

1.4 Basics of gain selection

The separation principle mentioned in the introduction states that the attitude inaccuracies due to estimator error and controller error are independent and additive. Since a chain is only as strong as its weakest link, there is no point in having a very different performance between the feedback control part and the estimator part, in particular as regards the acquisition time. Acquisition time is one of the main criteria in tuning both the controller and the estimator. This leads us to the recommendation to keep the order of the response time for the two chains similar.

Tuning of the the gains of the PD law and the reconstructor is done in partly heuristic ways. The methods used are described in more detail in the sections below. As a general rule, we will state that the robustness of the control is best served by 'conservative' gain settings, i.e. a controller which is as soft and slow as the required attitude control accuracy and acquisition time in a particular mode will allow.

1.5 Sensor quantization noise (MGM)

In the gyro-less mode, the magnetometer is the only sensor available to the control loop during eclipse. This magnetometer (MGM) has a coarsely quantized output withs steps which work out to some 0.5 degrees of angular attitude. This will tend to cause rough limit cycle behaviour, especially if the derivative of the MGM output is also used to estimate the velocity. This observation is borne out by simulation.

Possible problems caused by this noisy behaviour are excitation of the flexible modes of the solar panels, and reaction wheel overheating. Appendix A provides a simple reaction wheel thermal model which can be added to the simulation software.

Several options are available to filter the MGM quantization noise before it reaches the reaction wheel command. These include :

- put a separate filter on MGM output.
- use 'slow' reconstruction filter settings.
- use 'soft' control law gains.

The separate filter approach does not seem more optimal than slowing down the convergence of the reconstructor. Also, it requires a change to the code of the on-board software. Unlike a separate filter, the reconstructor at least does something sensible with the information implicit in the torque command history. This advantage breaks down only if the model used by the reconstructor is very different from reality, as discussed later. The separate filter approach has not been pursued any further. It must be very slow to make sense anyhow, which affects the control stability.

Both the other options leave the structure of the controller intact, changing numerical parameters only in the on-board database. These options will be examined in more detail in the remainder of this document.

The 'soft' control gains are another way of avoiding high variance in the torque commands. If no strict pointing requirements apply, using very conservative control gains seems like a good idea anyway.

1.6 Attitude excursions due to kinematic and inertial coupling

The control algorithms of the satellite AOCS are split into three independent single-axis controllers. The assumed independence holds up reasonably well when control errors and velocities are small. In slews, these simplifying assumptions may no longer hold, and large attitude excursions may occur. Problems of this nature have been seen in simulations; the exact cause of these problems is a subject of further study, but two candidates are inertial cross-coupling torques and kinematically inconsistent attitude and velocity measurements. A third candidate which may be checked for in design simulations is wheel torque limitation at higher wheel speeds, which will occur especially during slews.

inertial cross-coupling torques

In large slews, inertial cross-coupling between the axes is present. These cross-coupling torques will appear as disturbance torques to each individual single-axis controller. Attitude excursions will result from these disturbance torques if the controller is not able to adequately handle them. This inadequacy may take several forms :

- the disturbance torque estimator may be too slow to follow the variations in torque.

If in addition the feedback controller has soft gains, a large attitude excursion is needed to generate the required torque command.

- the disturbance torque estimator may have a badly damped response to torque variations.

This possibility should be ruled out by design. Pole-zero plots and simulated time histories of estimator state responses can be used to ensure adequately damped responses from the filter

- the disturbance torque estimator may be absent.

If no disturbance torque estimator is used, then the cross-coupling torques are not modelled in the estimator. Since the resulting velocity and attitude offsets do show up in the measured outputs, the filter has to cope with unmodelled disturbances. It is known that state reconstructors do not take kindly to this.

kinematically inconsistent attitude and velocity measurement

It may be that the problem is caused not so much by the 'disturbance torques', but by the fact that in some simulations the measured outputs for attitude and velocity are kinematically inconsistent. This can occur especially if attitude sensors are used which measure Euler angles about a particular axis, and velocity information is obtained by differencing components of a three-dimensional quaternion representation.

Most of the information contained in the quaternion in the simulations referred to was due to the attitude sensor anyway, and the solution proposed below is to reduce the filter accordingly to a filter which compares its state to a measured attitude only.

solutions

One solution proposed is to abandon the state reconstructor - PD law approach in favour of PID integrating control during slews. The integration would have to be reset or frozen for control errors larger than a certain value (i.e. at least for the slew axis), to prevent undue buildup or runaway. This solution is not favoured for reasons mentioned earlier in this chapter.

The second solution for the gyro-less mode is to try the simplest possible reconstruction filter, i.e. no augmented states to estimate disturbance torque and gyro drift, and only the attitude measurement as a reference output. This solution is sensitive to the wheel torque limitation at higher wheel speeds, since this limitation will appear as a disturbance torque to the estimator. Numerical values for this option are presented later.

The third solution is to augment the state with a disturbance torque estimator which converges quickly enough to make a useful contribution to the slew path accuracy, without attracting too much of the available information at the expense of the other two estimated states (attitude and velocity). Numerical values for this option are easily obtained, but have not been included in this note.

2 Selecting PD gains

2.1 General

The SAX control report gives a number of considerations for tuning the gains of the PD law. For the purpose of this memo, we will limit ourselves to the the case of fairly 'slow' gains. In that case, a purely continuous-time approach, disregarding sampling and control delay effects, is adequate. We will take as a basis the most simple satellite model in the continuous-time domain (later chapters will use the discrete time equations based on a 0.5 second sample time). Note the time derivative dot next to the state vector at the left hand side of the equation :

$$\begin{pmatrix} x \\ \dot{x} \end{pmatrix}^{\bullet} = \begin{pmatrix} 0 & 1 \\ 0 & 0 \end{pmatrix} . \begin{pmatrix} x \\ \dot{x} \end{pmatrix} + \begin{pmatrix} 0 \\ 1 \end{pmatrix} . u$$

We will introduce the ***PD*** feedback in non-dimensional form, with gains K_P and K_D. The actual gains P and D equal these gain factors, multiplied by the satellite inertia for that control axis :

$$u = -K_P . x - K_D . \dot{x} \quad \rightarrow \quad \begin{pmatrix} \dot{x} \\ \ddot{x} \end{pmatrix} = \begin{pmatrix} 0 & 1 \\ -K_P & -K_D \end{pmatrix} . \begin{pmatrix} x \\ \dot{x} \end{pmatrix}$$

The eigenvalues follow by solving the characteristic equation :

$$|\lambda . I - A| = \lambda^2 + K_D . \lambda + K_P$$

Comparing this formulation to the normal form for a second order characteristic polynomial in the Laplace variable s, we can characterize the eigenvalues by an undamped eigenfrequency and a damping factor :

$$s^2 + 2 . \zeta . \omega_o . s + \omega_o^2 = 0$$

$$K_P = \omega_o^2$$

$$K_D = 2 . \zeta . \omega_o$$

In a reasonably damped system, the first peak of a step response occurs after some $4/\omega_o$ seconds. If we select the first peak as a typical response time, and a damping factor of 0.7 as the basis of our design, we have as a design guide for an axis with satellite inertia I_{xx} :

$$\omega_o = \frac{4}{t_{first\,peak}}$$

$$P = I_{xx} . K_P = I_{xx} . \left(\frac{4}{t_{first\,peak}}\right)^2$$

$$D = I_{xx} . K_D = I_{xx} . 1.4 . \frac{4}{t_{first\,peak}}$$

2.2 Values used in existing design

The values used for the X-axis control gains in the gyro-less mode in the existing design were :

$$K_P = 0.00631 \qquad K_D = 0.300$$

The velocity gain K_D is much higher than could be expected for a normally damped design. The equations from the previous subsection would yield for the same K_P, with a damping of 0.7 :

$$K_D = 1.4\sqrt{K_P} = 0.111$$

The current gain is higher than this by a factor of almost 3 . This has several disadvantages :

- the system response is unnecessarily slow.
  (the 'tail' of the response converges very slowly due to the high damping)
- the noise transfer from velocity measurement to control torque is very high.

If we keep K_P as is, and reduce the damping factor to 0.7, the time to first peak of the step response can be calculated :

$$\omega = \sqrt{K_P} \qquad t_{first\,peak} = \frac{4}{\omega_o} = 50 \ seconds$$

This is a slow PD law. The next section gives an overview of a range of feasible PD gains, and the typical consequences of these gains.

2.3 New PD values

With the results of section 2.1 we can ~~make~~ define a family of gains which we expect to give good results. Table 2-1 below gives a few typical values. Figure 2-1 at the end of the text gives an impression of the variation of the gains with the design value of the first peak in the step response.

table 2 - 1 : Non-dimensional PD gains, for a damping factor of 0.7

$t_{first\,peak}$ (sec)	ω_o (rad/s)	K_P	K_D	*comment*
10	0.37	0.1369	0.523	
50	0.08	0.0063	0.111	Kp is current design value
75	0.05	0.0028	0.075	

2.4 Regulator-only Matlab simulation results

A small Matlab script was used to show the response of the PD law regulator with the old K_D gain and with the gain adapted to a damping of 0.7, both for the same value of the proportional gain K_P. Figure 2-2 at the end of the text shows the responses of both settings to an initial attitude offset. The improvement with the adapted gain is obvious. Similar simulation results were obtained at Alenia during recent visits of the FSS consultants there.

Further regulator-only Matlab simulation results are presented in later sections of this note as a comparison to the results including the estimator in the loop. These results are based on the gains in table 2-1 .

3 General filter setting strategy

Optimal settings for the reconstructor are calculated for SAX with LQE theory, using the Riccati equation. Small heuristic modifications to the values found have been made in the past. The LQE optimization process requires certain input parameters, viz. the expected system noise and measurement noise values.

An attempt can be made to make realistic estimates of both values. This has proven difficult in the past. For the satellite ISO, an extensive performance simulation survey was made trying to match the performance predictions from LQE methode to the simulation results for a variety of idealised and practical conditions (control delay, wheel torque inaccuracy, star tracker delay, inertial cross-coupling, measurement quantisation, scaling errors and random noise). It was found that system input noise values in the order of 1.5 RWL torque step were needed to match LQE predicted variance to the simulation results (see ISO-FO-TN-119, section 5.2.1) . No obvious physical justification has been found for this result.

The tuning method in ISO has been to consider the design noise values not as a representation of the actual noise values, but just as non-dimensional weighting parameters for the various noise contributions. This way of using LQE design is also advocated in literature (e.g. see Franklin, Powell e.a., 'Digital Control of Dynamic Systems') . Performance is judged and tuned on the basis of simulations, seeking a compromise between good satellite limit cycle and reasonable filter convergence behaviour. It was also noted that the reconstructor design has one degree of freedom less than the total number of system and measurement noise values: scaling all noise values with the same factor does not yield a different reconstructor.

A first impression of the estimator convergence behaviour may be obtained from the eigenvalues of the estimator matrix A-L C A . The discrete eigenvalues can be converted to equivalent s-plane natural frequencies and damping factors using the Matlab function 'ddamp' . This routine uses the following equations for the equivalence between discrete and continuous time domain :

$$s = \frac{\log(r)}{\Delta T}$$

$$\omega_o = |s|$$

$$\zeta = -\cos\left(atan\left(\frac{\mathrm{imag(s)}}{\mathrm{real(s)}}\right)\right)$$

In the next chapter we will be using this same method to tune the SAX estimator values. In particular, we will use a basic system noise value of 1 and scale the other noise values relative to this basis (i.e. we will not attempt to use realistic noise values), and we will use the typical convergence time according to the equations above as the basic tuning criterion.

4 A two-state, one output no-gyro estimator

4.1 Number of reference outputs

In the no-gyro mode, the only reference output available to the filter is the attitude relative to the magnetic field, as measured by the magnetometer (MGM). The normal filter structure in SAX has two reference outputs, one for the attitude and one for the velocity. We now have the option of 'simulating' the velocity measurement by taking the derivative of the attitude data, or by omitting the second output from the filter design calculations altogether. The second option seems the cleanest one. Full-order trial simulations at Alenia have confirmed that it also gives better results in practice. In particular, the slew path turned out to be more accurate using the single output structure. Constructing a simulated velocity output has the following potential disadvantages :

- the simulated velocity and the attitude information may be inconsistent.
- the weighting factor between the attitude and velocity outputs must match.

As to the first point, it has been proposed to derive the velocity information from quaternion data, and the attitude data from MGM. The potential problem to the closed-loop control may be that the filter gets velocity data which is not the derivative of the attitude data. This might be kinematically more correct as a whole, but the estimator may react quite badly, since estimators generally do not take kindly to differences in structure between their implicit model and the real world model.

As to the second point, the simulated velocity measurement is essentially the derivative of the actual attitude measurement. The noise values of the two are directly coupled through a differencing operation. It is likely that optimum results are obtained when the weighting factors for the two outputs are matched accordingly in the filter tuning design phase. It would seem easier and less prone to error to accomplish this in the filter structure proper.

4.2 Filter values for a second-order, one output filter

The simplest reconstructor we can devise for the no-gyro mode of the SAX AOCS has an internal model with effectively only two states (attitude and velocity), and one output (magnetometer MGM). Since no accuracy requirements apply, the augmented states for the disturbance torque and the gyro drift may be omitted.

This reduced reconstructor is assumed to have only one system noise input, taking the form of an unknown torque, and one measurement output noise, representing mainly the quantization noise of the MGM. These are two design values only. The introductory section on calculating reconstruction filter settings mentioned that there is in fact one degree of freedom less in the LQE design process than appears at first sight. This leaves in our case only one degree of freedom in the reduced LQE design, viz. the ratio between system noise and MGM measurement noise. Arbitratily setting the system noise to one, we get the following L matrices for various MGM noise values. The calculation was done with the Matlab function DLQE, which is equivalent to the MatrixX function DESTIMATOR (old version) or ESTIMATOR with digital system arguments (new object oriented version). These functions yield an estimator design for a 'current' output, i.e. the estimate for a given sample time includes the measurement

data for that same sample time (zero data processing delay). This is the case applicable here, and in general the most useful case in practice. Note that most theoretical books will describe the simpler case for the 'previous output' estimator first, and often leave it at that.

Table 4-1 below gives some results. The L matrix calculated for an MGM noise factor of 45 closely corresponds to the values used in earlier Alenia design simulations. Figure 4 - 1 at the end of the text shows a graph of $t_{peak} = 4 / \omega_o$, as a function of the design value for sigma MGM.

table 4 - 1 : Filter values for an estimator with two states and one output (for measured attitude)

MGM noise	L matrix (2 * 1)	lowest natural frequency (rad/s)	approx. first peak (sec)
7.5	0.22742 0.05860	0.37	11
15	0.16682 0.03043	0.26	15
45	0.10003 0.01054	0.15	27
100	0.068265 0.004826	0.10	40
155	0.055212 0.003135	0.08	50
355	0.036833 0.001382	0.05	75

NOTES : All estimators have a damping of 0.71 .

t_{peak} is calculated as $4 / \omega_o$.

4.3 Regulator plus estimator, Matlab simulation results

4.3.1 Types of run

Matlab simulations were run to test the convergence of the regulator and estimator from offsets in initial condition, and after a spike in the MGM output. Responses are shown for the following signals :

- attitude.
- velocity.
- torque command.

line types in attitude / velocity plots

The attitude and velocity are shown in three line types. The solid line is the actual attitude (c.q. velocity) response of the full closed system, i.e. with both estimator an regulator in place and having an initial offset. This represents the case where the actual attitude has an initial offset, which is not known the estimator (estimator not initialised to a known value).

The chain dotted line applies when the initial attitude is known to the estimator, i.e. the estimator has converged, and the estimator error will remain zero from then on. The chain dotted line therefore is also the response *without* the estimator in the loop, i.e. with the regulator acting directly on perfect measurements. This we will call the 'regulator only' response.

The dotted line, finally, gives the response of the estimator error, i.e. the difference between the estimator and the actual state. This response is, in principle, independent of the regulator response.

line types and dimensions in torque plots

The torque command is also shown in three line types. The solid line once again is for the case of a full closed loop, i.e. with both estimator and regulator active. The chain dotted line is for the 'regulator only' case. The dotted line is for the full closed loop case, but gives the P term only. This gives some information on the separate effects of the attitude and velocity feedback on the torque demanded. The torque commands themselves are non-dimensional. To give a feel for their values, the torque plots are scaled to represent dimensional commands (in Nm), for an axis with a moment of inertia of 1600 kgm2, and for an initial attitude offset of 1 degree, c.q. an MGM spike of 1 degree during 1 sample period.

4.3.2 Convergence after attitude offset

Figures 4-2 through 4-6 give Matlab-simulated responses to an initial attitude offset.

figure 4-2 responses for 'fast' regulator and 'fast' estimator

Figure 4-2 gives the responses for 'fast' regulator and 'fast' estimator settings. The settings are characterised by 'first peak' values of 10 seconds, in the sense defined in previous chapters, Ch. 2 for the regulator and Ch. 3 for the estimator.

The 'closed loop' case shows a first peak after 10 seconds, as expected. There is an overshoot of nearly 60 % due to the combined response of regulator and estimator. The chain dotted 'regulator only' case (estimator properly initialised or converged) obviously has a very crisp and well-damped response. The estimator-error response appears even faster, but less well damped. This is not due to a difference in damping or eigenvalue between regulator and estimator (those are identical), but due to different eigenvectors. The result is a different response to this particular initial condition than for the regulator. An other simulation with an initial velocity offset, not shown here, does give nearly identical responses from both the regulator and the estimator.

The torque for these settings peaks at almost 4 Nm, both for the closed-loop case and for the regulator-only case. This is many times higher than the maximum reaction wheel torque in SAX, and clearly undesirable behaviour.

figure 4-3 responses for 'fast' regulator and 'slow' estimator

One way of reducing the commanded torque is by slowing down the convergence of the estimator. Figures 4-2.b show the results. The overshoot in the 'closed loop' case is nearly 30 % . The commanded torque is reduced to a maximum of 0.6 Nm in the 'closed loop' case. However, there is no slowing down of the response, and consequently no torque reduction in the 'regulator only' case. In other words, if the filter has converged or has been properly initialised, the commanded torques are still extremely high.

figure 4-4 responses for 'slow' regulator and 'fast' estimator

Another way of reducing the commanded torque is by slowing down the regulator, without slowing down the estimator. Figure 4-4 shows the results. Contrary to the reverse case just discussed, slowing down the regulator settings reduces the commanded torques considerably in the 'regulator only' case, i.e. for converged or properly initialised estimator. The initial torque is in fact reduced to the order of the maximum wheel torque. Somewhat surprisingly, the torque commands remain in the much higher 0.6 Nm range for the full 'closed loop' case. The torque plot shows that this torque is due to mostly to the response in the velocity estimate.

figure 4-5 responses for 'slow' regulator and 'slow' estimator

The most obvious way of reducing the commanded torque is by slowing down both the regulator and the estimator to the same order of magnitude. Figure 4-5 shows the results for slowing down both to a 'first peak' time of 50 seconds. The behaviour is quite similar to that shown in figure 4-2, and discussed above; only, everything happens at a lower rate, and the torques and velocities are accordingly lower. The maximum torques are now in the 0.1 to 0.15 Nm range, both for the 'regulator only' and for the 'closed loop' case. The factor of 5 increase in typical response time has resulted in a similar factor in torque reduction.

figure 4-6 even slower regulator and estimator

For completeness' sake, figure 4-6 shows the same response as in figure 4-5 for an even slower setting of both regulator and estimator. Both now have a typical first peak time of 75 seconds. This is a factor of 1.5 slower than figure 4-5. The resulting torque reduction is from a peak 0.13 Nm to less than 0.06 Nm, a reduction by a factor of more than 2 .

MatrixX results

Simulations similar to the Matlab simulations reported here were done during the visits of the FSS consultants at Alenia. The results were similar to those reported here.

4.3.3 Response to a spike in MGM output

A rough limit cycle behaviour was first encountered in simulations of a pointing on the MGM only. The behaviour is caused by the sudden transitions between one transition step and the next. As a first idealised assessment, we will study in this section the response of the controller to a single spike in the MGM output. We will consider only the improvement between the cases of 'slow' regulator and 'fast' estimator, and the case where both are equally slow.

figure 4-7 MGM spike responses for 'slow' regulator and 'fast' estimator

Figure 4-7 shows the response to a single MGM spike of 1 degree, a very coarse quantisation step transition lasting only a single sample time interval. The estimator responds by a step of 0.25 degrees in the attitude, and 0.07 deg/sec in the velocity estimate. The control law responds with a torque step of 0.26 Nm, i.e. more than full torque. This torque is mainly due to the velocity gain, which is much larger than the proportional gain for slow regulator settings (see table 2-1).

figure 4-8 MGM spike responses for 'slow' regulator and 'slow' estimator

Figure 4-8 shows the same responses as figure 4-7, but this time with a 'slow' estimator. The response in estimated attitude is down to 0.05 degrees, and the response in estimated velocity down to some 0.003 deg/sec. The torque step is down to less than 0.02 Nm. About half of this is due to the velocity gain.

4.3.4 Conclusion on Matlab simulations

We can conclude that slowing down the estimator is an effective way of reducing the effects of steps and MGM spikes. The improvement will be less dramatic in actual practice, since the MGM signal is usually not a spike, but a result from crossing a quantisation border. Slower system response may imply that the signal will persist for longer than a single sample period, which will increase the response of the estimator in proportion.

4.4 Regulator plus estimator, Alenia trial simulations

4.4.1 Settings used in trial simulations

A number of trial simulations was performed on the simulation tool at Alenia. The settings used were very similar to those proposed in this note. In the terms of tables 2-1 and 4-1, the settings were :

table 4 - 2 : Non-dimensional PD gains in Alenia design simulations			
$t_{first\ peak}$ (sec)	ω_o (rad/s)	K_P	K_D
128	0.032 0.077	0.0025	0.111
note :	**The damping factor is larger than 1.** **'omega' column now gives eigenvalues,** **'peak time' is 4/lowest eigenvalue.**		

table 4 - 3 : Filter values similar to Alenia design simulations			
approx. first peak (sec)	*lowest natural frequency (rad/s)*	*MGM noise*	*L matrix (2 * 1)*
55	0.0725	190	0.05 0.0025

The settings for K_p and K_d do not follow the recommendations in this note. The value of 0.111 for K_d is a value which matches one of the other known settings for K_p, 0.0631, if we apply the equation for optimum damping given earlier, $Kd = 2.\zeta.\sqrt{(K_p)}$. The current settings give a very slow regulator response.

The setting of the L matrix is much closer to an optimum setting. The 'typical response time' is 55 seconds. This seems like a decent setting, except that it is much quicker than the effective setting of the regulator, which seems unnecessary.

4.4.2 Matlab replay of trial simulation settings

Figure 4-9 gives a Matlab-simulated response to an initial attitude offset, using the settings used in the Alenia trial simulations. The response is similar to the reponses given in figures 4-7 and 4-8 for 'slow' and 'even slower' settings. The very slow regulator response due to the badly matched K_d gain is readily apparent.

4.4.3 Results of the trial simulations

Some results of the Alenia trial simulations are presented in 'GSM design status summary No.2' dd. 24 March, 1995, and 'No.3, dd. 28 March 1995. One observation made in 'No.2, near the top of page 2 is that even with a partial reset of the estimator when the magnetic torquers are switched on or off, both the actual attitude and the estimated velocity take some time to settle after such a switch. This is attributed to a slew needed to acquire the new target attitude, combined with heavy filtering in the estimator.

If the measured attitude is taken as the new target, no slew towards a new target attitude would seem to be needed. Also, no filtering is applied to the torque command input to the estimator, so any deliberate slew should be represented correctly in the velocity estimate. However, disturbance torques (including magnetic torquer torque and wheel friction) will cause a slew to a new equilibrium attitude, which is offset from the target. This offset may be noticeable if the K_p gain is low. As a rough order of magnitude estimate, with a disturbance torque of 0.007 Nm and a typical K_p gain of 0.0025, we have a static offset of :

$$K_P . I_{xx} . e = T_{dist}$$

$$e = \frac{T_{dist}}{K_P . I_{xx}}$$

$$e = \frac{0.007}{0.025*1600} = 0.0075[rad] = 0.1°$$

The velocity estimator is unaware of these disturbance torques, and hence will not be able to interpret this slew correctly. If the closed loop control system is very slow, erroneous velocity estimates may persist for quite some time. Dr. Karsten has proposed to avoid the output step and accompanying re-initialisation of the estimator altogether, by correcting the MGM output for the known effects of torquer actuation (FSS-SAX-LK-9513, 'Comment on GSM design status summaries 1..3', dd. 95 04 05). If this route is not chosen, and the problem is indeed caused by the disturbance torques, then it may be solved by re-instating the third state of the estimator. This will maintain an estimate of the disturbance torques (mainly those due to reaction wheel friction) through the partial re-initialisation.

5 Other estimator options

5.1 Discarding the estimator

The internal dynamics of the reconstructor is of help only if it is a reasonable model of the actual satellite. If the two differ too much, there will come a point when using the model no longer improves the performance. The choice is then to either discard or improve the estimator. Important effects which are presently not modelled in the reconstructor include :

- wheel saturation (in particular when the wheels are loaded to high velocities).
- inertial cross-coupling between axes (in particular at high slew velocities).

Ways of improving the estimator's handling of these effects will be discussed below. The first option however is to dispense with the reconstructor as a predictive model altogether. The reconstructor can be modified into a simple low-pass or all-pass filter. The torque noise suppression may be helped by using very 'soft' gains in the control law. One of the control problems, however, is that the velocity measurement is not always available. Estimating the velocity from the current and previous MGM readout only seems unlikely to give satisfactory results. Some form of filtering will be needed, and it might as well be done by a filter with some form of internal model, which brings us back to the estimator.

5.2 Adding disturbance torque estimate

If slew path offsets due to inertial cross-coupling during large slews is perceived as the most serious problem, then a possible solution is to add the disturbance torque estimator back into the estimator equations. This increases the number of estimator design paramters from one (as in the previous chapter) to two. The second design parameter is the ratio between the assumed disturbance torque noise, and the assumed system input noise. The latter is always set to 1, for reasons explained in the previous chapter. This extra design parameter governs the acquisition rate of the disturbance torque estimate, without appreciably affecting the acquisition rate of the other states.

The normal with-gyro design uses values for this parameter, which give the disturbance torque state a typical acquisition time of several hundreds of seconds. This is easily reduced to the order of less than one minute if desired. With such fast acquisition, the disturbance torque estimator is able to follow the variations in cross-coupling torque during slews. This will give more accurate tracking during the slew, much like an integrating controller would. Allowing the estimator to put energy into this state is a more accurate model of what is actually happening than ignoring the cross-coupling torque. This in itself may give less systematic errors on the other states. Since the off-track devation during slews is currently not seen as a serious problem, this possibility has not been numerically elaborated or simulated in the present note.

5.3 Limiting the estimator errors

In many cases, the modelling inaccuracies and non-linearities are most obvious for large errors and velocities. In such cases, there is the option of limiting certain states to maximum values, or of resetting the filter continuously to the measured values while the torque command is larger than, say, twice full torque. This is similar to the limiting which is usually applied to integrating controllers to prevent integrator runaway.

5.4 Modelling wheel saturation

A 'better' estimate of wheel torque is already available in the RWS health checking. If wheel saturation is perceived as a serious problem, a simple and effective solution would be to feed this torque prediction to the estimator, instead of the commanded torque. This would entail a real, if small, modification to the flight software.

5.5 Using wheel tacho data as a velocity measurement

Under certain assumptions, it is feasible to use the output of the wheel tacho's as an estimate of the satellite angular velocity. The main assumption is that there is conservation of angular momentum (i.e. no external torques), and that the initial angular momentum is known, e.g because the satellite body is assumed initially stationary. In that case, all initial angular momentum is contained in the wheels, where the tacho's can measure it.

wheel velocity reference

There is a catch in determining the reference velocities for the wheels, which has been missed in some of Alenia's earlier trial simulations for pointing during eclipse. The catch is relatively easy to repair, however. The referenced simulations assume as mentioned before, that at the start of eclipse, the satellite body is more or less stationary. The angular momentum contained in the wheels at this moment is therefore taken as a reference for further pointing. However, at eclipse entry an intentional slew is commanded towards the magnetic field vector. After this slew, the total angular momentum will still have roughly the same inertial value and direction as before, but it will point to a different direction in the satellite. The distribution over the wheels will therfore also be entirely different. Therefore, the angular momenta of the individual wheels cannot be kept at the same reference value as before the slew. The fix is obvious and in principle not complex : at eclipse entry the wheel angular momenta must be combined into a single vector. This vector will remain inertially fixed. As soon as the slew quaternion towards the new target (the magnetic field vector) has been determined, the angular momentum vector can be transformed from its current location in the satellite body to the location it will have at the end of the slew. This allows a new decomposition into individual wheel velocities. These new components now become the new reference values. These reference values can probably already be used during the slew, although this is in principle not accurate.

5.6 Modelling inertial cross-coupling

Modelling of the inertial cross-coupling requires adding to the software some essentially non-linear, three-axis model terms, in addition to the three independent linear single-axis models currently used. Calculating the cross-torques, and adding them to the wheel torque estimates fed as an input to each of the single-axis estimators, would seem straightforward in principle. It does require some extra on-board calculation time, and it also interlinks the control of the three axes. This might make for a less robust and predictable setup. Also, it does not protect us from cross-couplings due to the velocity of the magnetic field, which is not observable when only MGM data is used.

The cross-coupling between axes is the non-linear function $\omega \times H$, of the angular velocity and the total angular momentum. The angular velocity for every axis follows from the filter states. With some knowledge of the satellite's moments of inertia, the angular momentum can also be calculated from the angular velocity. The next subsection will deal with a more accurate way of estimating the total angular momentum.

5.7 An estimator state for total angular momentum

When introducing inertial cross-coupling to the estimator, a further improvement can be made by maintaining an estimate of the total angular momentum in the satellite (handwritten memo Dr. L. Karsten, dd. 95-03-09) . This total angular momentum estimate is added as an extra state to the estimator. The new state takes the place of one of the existing states (disturbance torque or gyro drift, both unused in the gyro-less mode) ; thus keeping software changes to a minimum. The wheel tacho acts as a second output in addition to the magnetometer, effectively replacing the gyro. In this sense, this solution is a combination of the solutions in the previous two subsections.

The estimator model equations in Dr.Karsten's memo use the *total angular momentum* as a third state. The input is expanded with an inertial cross-coupling term. The equations are shown for the X-axis, i.e. with inertia I_{xx} :

$$u = \begin{pmatrix} \frac{M_{RWL}}{I_{xx}} & \frac{\omega \times H_{total}}{I_{xx}} \end{pmatrix}$$

The tacho output is constructed from the states in the following way (see also 'a note on signs and dimensions' below) :

$$y_{tacho,k} = \Delta T \cdot \omega_{RWS} = \Delta T \cdot \frac{H_{RWS}}{I_{xx}} = \frac{\Delta T}{I_{xx}} (H_{total} - H_{body})$$

$$y_{tacho,k} = \Delta T \cdot \frac{H_{total}}{I_{xx}} + \Delta T \cdot \dot{e}_k + \frac{\Delta T^2}{2} \cdot \frac{M_{RWS}}{I_{xx}}$$

A completely equivalent, and perhaps simpler formulation of this three-state estimator model follows by applying the following linear transformation to the system state :

$$x' = S.x \qquad S = \begin{pmatrix} 1 & 0 & 0 \\ 0 & 1 & 0 \\ 0 & I_{xx} & 1 \end{pmatrix}$$

The interpretation of the states is :

$$x = \begin{pmatrix} e \\ \dot{e} \\ H_{total} \end{pmatrix}$$

$$x' = \begin{pmatrix} e \\ \dot{e} \\ H_{total} + I_{xx}\dot{e} \end{pmatrix} = \begin{pmatrix} e \\ \dot{e} \\ H_{RWL} \end{pmatrix}$$

The system equations are transformed as follows :

$$\dot{x} = A.x + B.u$$

$$y = C.x + D.u$$

$$S^{-1}.\dot{x}' = A.S^{-1}.x' + B.u$$

$$y = C.S^{-1}.x' + D.u$$

$$S.S^{-1}.\dot{x}' = S.A.S^{-1}.x' + S.B.u$$

$$y = C.S^{-1}.x' + D.u$$

The system expressed in the new state x' becomes :

$$\begin{pmatrix} e \\ \dot{e} \\ H_{RWL} \end{pmatrix}_{k+1} = \begin{pmatrix} 1 & \Delta T & 0 \\ 0 & 1 & 0 \\ 0 & 0 & 1 \end{pmatrix} \cdot \begin{pmatrix} e \\ \dot{e} \\ H_{RWL} \end{pmatrix}_k + \begin{pmatrix} -\Delta T^2 & -\Delta T^2 \\ -\Delta T & -\Delta T \\ -\Delta T.I_{xx} & 0 \end{pmatrix} \cdot \begin{pmatrix} \frac{M_{RWL}}{I_{xx}} & \frac{\omega \times H_{total}}{I_{xx}} \end{pmatrix}_k$$

$$y = \begin{pmatrix} 1 & 0 & 0 \\ 0 & 0 & \frac{\Delta T}{I_{xx}} \end{pmatrix} \cdot \begin{pmatrix} e \\ \dot{e} \\ H_{RWL} \end{pmatrix}_k + \begin{pmatrix} 0 & 0 \\ \frac{\Delta T^2}{2} & 0 \end{pmatrix} \cdot \begin{pmatrix} \frac{M_{RWL}}{I_{xx}} & \frac{\omega \times H_{total}}{I_{xx}} \end{pmatrix}_k$$

This formulation shows that the third state is independent of the other two states. It is a separate estimator for the angular momentum in the reaction wheels only, with the tacho as a separate dedicated output, and the wheel commands as the only input.

Note that the reverse is not true; the other two states are not independent of the state of the wheel angular momentum estimator, since that state enters in the calculation of H_{total} via $H_{RWL} - I_{xx}.\dot{e}$. In a wider sense, the third state does depend on the first two, since the control law calculates the wheel commands from the first two states.

a note on signs and dimensions

It is noted that the third state in the original formulation is not non-dimensional, unlike the first two states. it also, again unlike the first two states, does not have the 'error' sign convention.

The reference output shown in the original formulation is dimensioned to be similar to a rate integrating gyro output, i.e. the reference output is equivalent to an angular displacement of the satellite (not the reaction wheel). This requires a conversion before feeding the tacho output to the estimator's L matrix. The conversion consists of multiplying the tacho ticks by the number of radians per tick mark and the wheel inertia, and dividing by the assumed satellite inertia.

tuning the L matrix for the extra state

The convergence of the extra state can be tuned with pole placement by hand, since it is a simple independent first order digital filter. The same result can be obtained on that single order estimator by introducing a new ratio of two design variables, viz. an extra system noise input, acting only on the new state, and a measurement noise value for the tacho output. And again the same result can be obtained by adding the new noise input and measurement noise to the third order system shown above. In the latter case, we find the following L matrix :

$$L = \begin{pmatrix} l_{11} & 0 \\ l_{21} & 0 \\ 0 & l_{32} \end{pmatrix}$$

The values for l_{11} *and* l_{21} can be taken directly from table 4-1. Only the value of l_{32} depends on the tacho noise value. The table below gives some values. Note that the system can be transformed back to the 'total angular momentum' interpretation of the third state if desired. The L matrix will then no longer have three zeros.

table 5 - 1 : Filter values for angular momentum estimator			
tacho noise ratio over system noise	**l_{32}**	**natural frequency (rad/s)**	**approx. first peak (sec)**
10 / Ixx	0.98 * Ixx	0.1	40
5 / Ixx	0.19 * Ixx	0.2	20
2 / Ixx	0.44 * Ixx	0.5	8

6 Validation

6.1 Simplifications in initial design analysis

The design process described so far has the following simplifications :

- it is based on linear system theory.
- wheel saturation etc. is not part of the initial analysis.
- cross-coupling between satellite axes is initially ignored.
- PD gains are initially designed in the continuous-time domain.
- control delay is not addressed.
- rigid satellite model is used, no flexible panels.

The tools used are simplified linear analysis and simulations.

6.2 Design and verification simulations

Confidence in the stability and robustness of the control loop is gained from design simulations. These build up from simple Matlab or MatrixX to full complexity design simulations, with and without modelling flexibility etc. .

Part of the verification is probably done by systematic verification simulations, with well defined 'worst cases' .

6.3 Formal proof of stability and robustness

The final and formal check on the stability in SAX control rests on a Matlab analysis program, plus a set of criteria, laid down by J. Kouwen of FSS. The analysis program establishes the closed loop system gain and phase margins, at the frequency of the lowest structural mode of the solar panels. The criteria require margins with a safety factor for effects not included in the Matlab calculations. These include control system delay and various system non-linearities, which are for the most part also covered by the design simulations.

7 Observability problems

7.1 Assumptions

Most of this note only addresses closed-loop control. However, it may be worthwhile to record here a number of assumptions which are implicit in the solutions proposed for the gyro-less safe mode. These assumptions include :

- at mode entry, the total angular momentum is zero.
- the magnetic field vector always differs more than 10 degrees from the Sun vector

The first assumption is of course not true, but it is the best assumption available, and without it control becomes very difficult. The assumption is based on the premise that the previous history was not disastrous, and that the wheels have been kept reasonably unloaded. An alternative assumption is that the satellite body angular momentum is zero.

The second assumption is needed for a successful application of the strategy which we will briefly discuss below.

7.2 Keeping the X-axis aligned with the magnetic field in eclipse

There is a requirement that the X-axis of the satellite shall not point directly into the Sun. During eclipse, the magnetic field vector is the only observable attitude information, and it will not point directly into the Sun. The only guarantee that the X-axis will not look at the Sun is by keeping it aligned with the magnetic field vector. Keeping any other vector in the satellite aligned with the magnetic field (an obvious candidate would be the direction which the vector had at eclipse entry) opens the possibility that the X-axis rotates about that vector, directly into the Sun. The solution adopted necessitates an intentional slew at eclipse entry.

7.3 Hold-on-wheels about the X-axis in eclipse

No measured attitude information is available about the magnetic field vector during eclipse. However, if no control is exercised around this axis, the reaction wheels will spin down around this axis on their own friction. The angular momentum in the reaction wheels will be transferred to the satellite body. Some form of control is needed to keep the wheels at the same angular velocity. The method now envisaged, is as follows :

- assume a reference for the angular momentum of the wheels at zero satellite body velocity.
- measure the angular momentum currently in the wheels by tacho.
- subtract the two, and calculate the satellite body velocity from this, using the ratio between wheel inertia and satellite body inertia. Use this as a 'velocity measurement' for the X-axis.
- integrate the 'velocity measurement' into an 'attitude measurement'.

This method, and some details on determining the reference value, was already discussed in the previous chapter on 'estimator options'.

8 Conclusion

The simplest solution to the gyro-less closed loop control is a combination of 'soft' PD regulator gains and a 'slow' state reconstructor. This estimator will have two states, and one reference output, viz. the measured attitude. It seems logical to match the response time of the attitude estimator to the response time of the regulator. Both converge independently, and the actual attitude will have converged only if both the regulator and the estimator have converged.

The convergence time of the current regulator for the X-axis is extremely slow. It can be made faster, giving a typical response of 50 seconds, if the D gain (velocity feedback) is reduced to better match the existing P gain.

Convergence of the actual attitude is never faster than the regulator will allow. This indicates that from a time response point of view, it is not very useful to have an estimator convergence much faster than the regulator response. The reverse is not necessarily true; when the estimator has converged, the deterministic control response will be identical to the regulator response, regardless of how long it took the estimator to converge. Nevertheless, it also does not seem to be very useful to make the regulator much faster than the estimator. As a result, we find that it is logical to tune the regulator and estimator to have similar response times.

A convergence time of 50 to 75 seconds would seem a reasonable design value, if the aim is to have a very slow, but robust controller which is insensitive to noise and quantisation steps. Relatively large 'quasi-static' offsets must are then accepted in the presence of disturbance torques and inertial cross-coupling. Design values and results of idealised simulations are given in this note for such design values. The torque response of these simulations indicate that torque levels will stay below maximum wheel torque under most pointing conditions, when steps or spikes below 1 degree of arc are encountered.

It is proposed to attempt full order simulations with these settings, for a number of conditions. If the results of these full-order simulations are satisfactory, a final check on stability margins can be made with the analysis software developed at FSS for checking the SAX control algorithms.

Problems of a more fundamental nature than these closed-loop control problems are expected to occur under adverse conditions. A possibility to counter some of these problems by maintaining an on-board estimate of total angular momentum has recently been proposed by Dr.Karsten. It is briefly discussed and commented on in this note.

FIGURES

figure 2-1 : PD control gains as a funtion of desired response time.

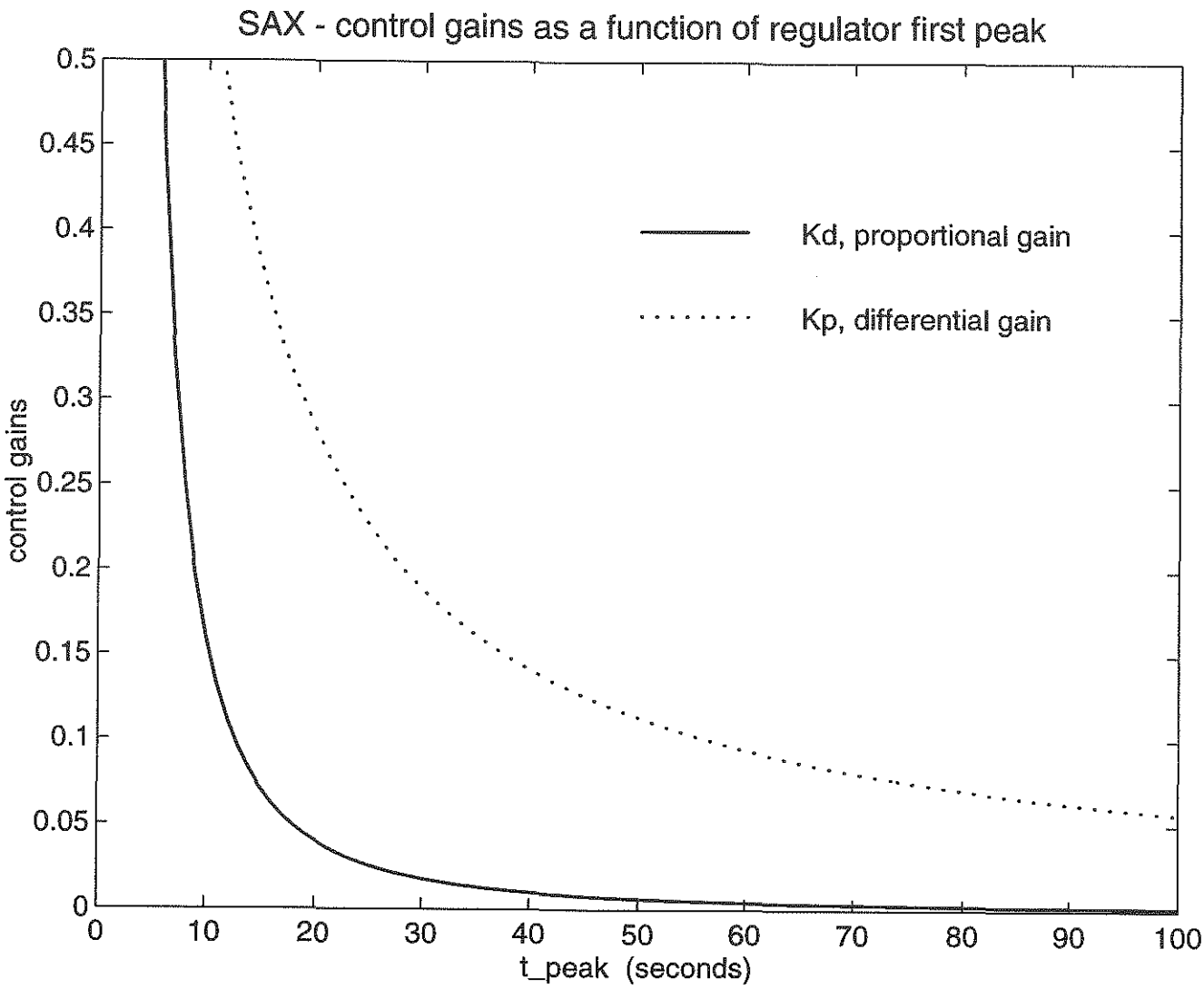

figure 2-2 : Initial attitude response for two settings of velocity gain in PD law.

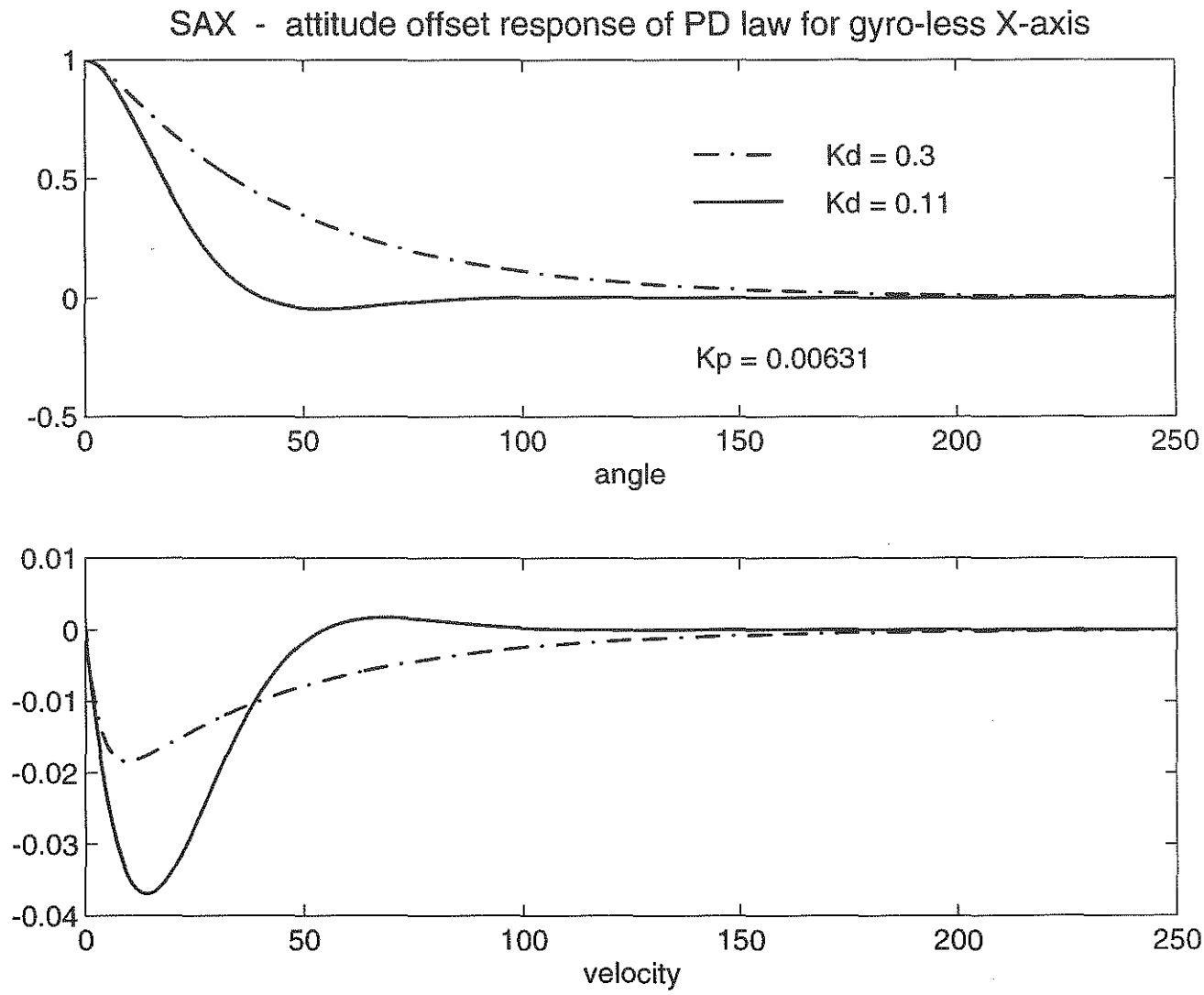

figure 4-1 : Estimator response : first peak as a function of design noise MGM.

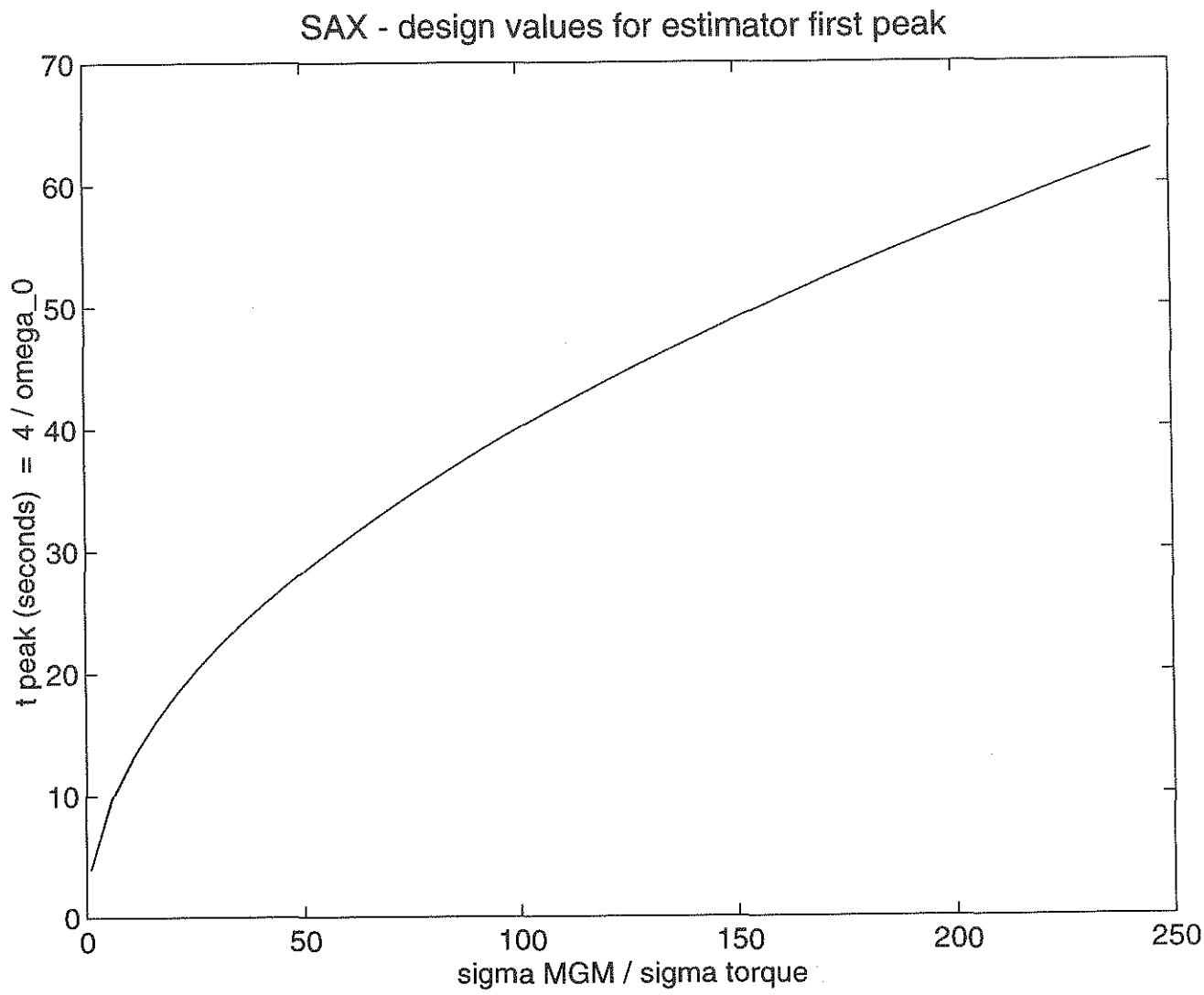

figure 4-2 : Convergence after initial attitude offset.
'fast' regulator
'fast' estimator

(figure 1 of 3)

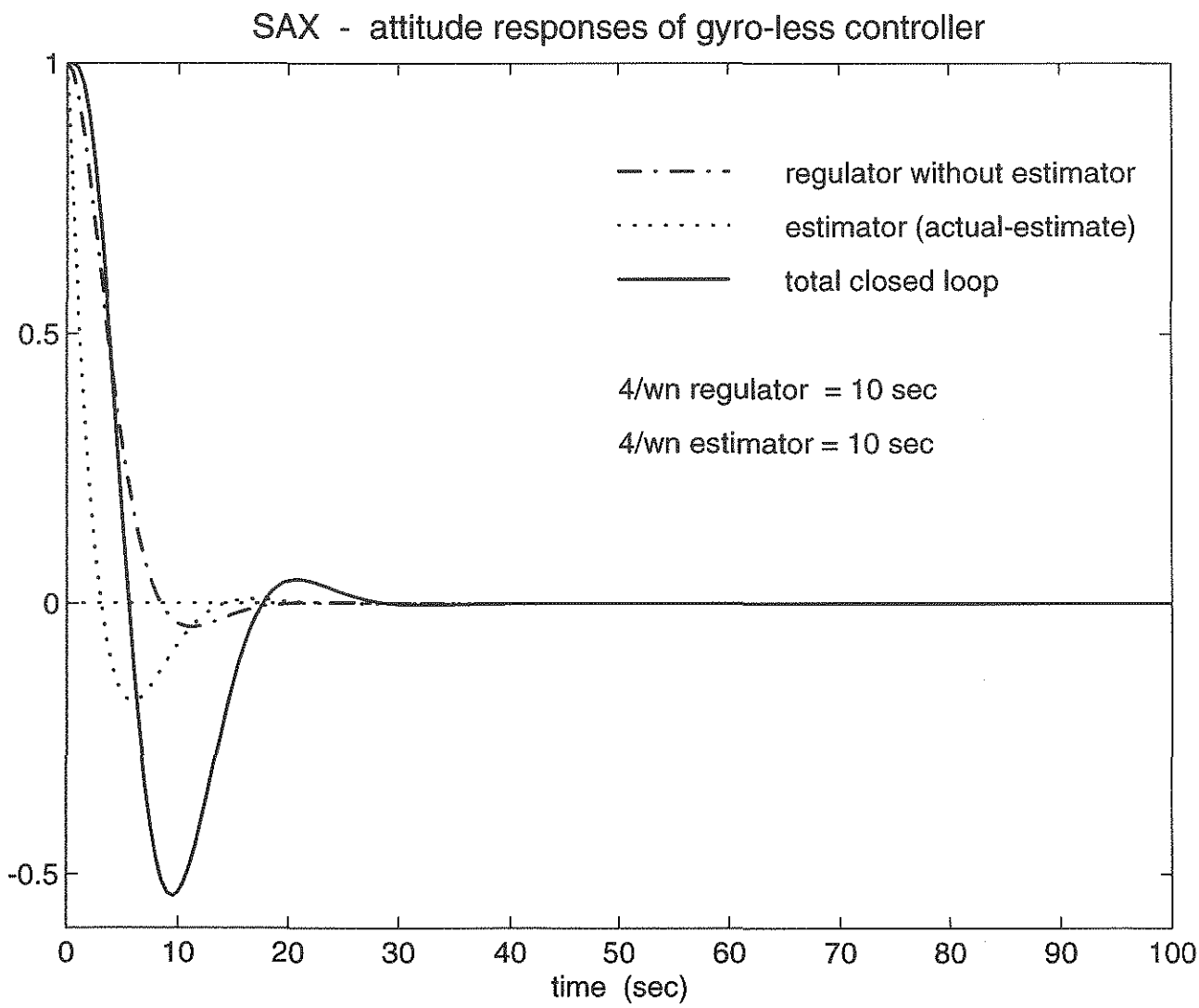

figure 4-2 : Convergence after initial attitude offset.
'fast' regulator
'fast' estimator

(figure 2 of 3)

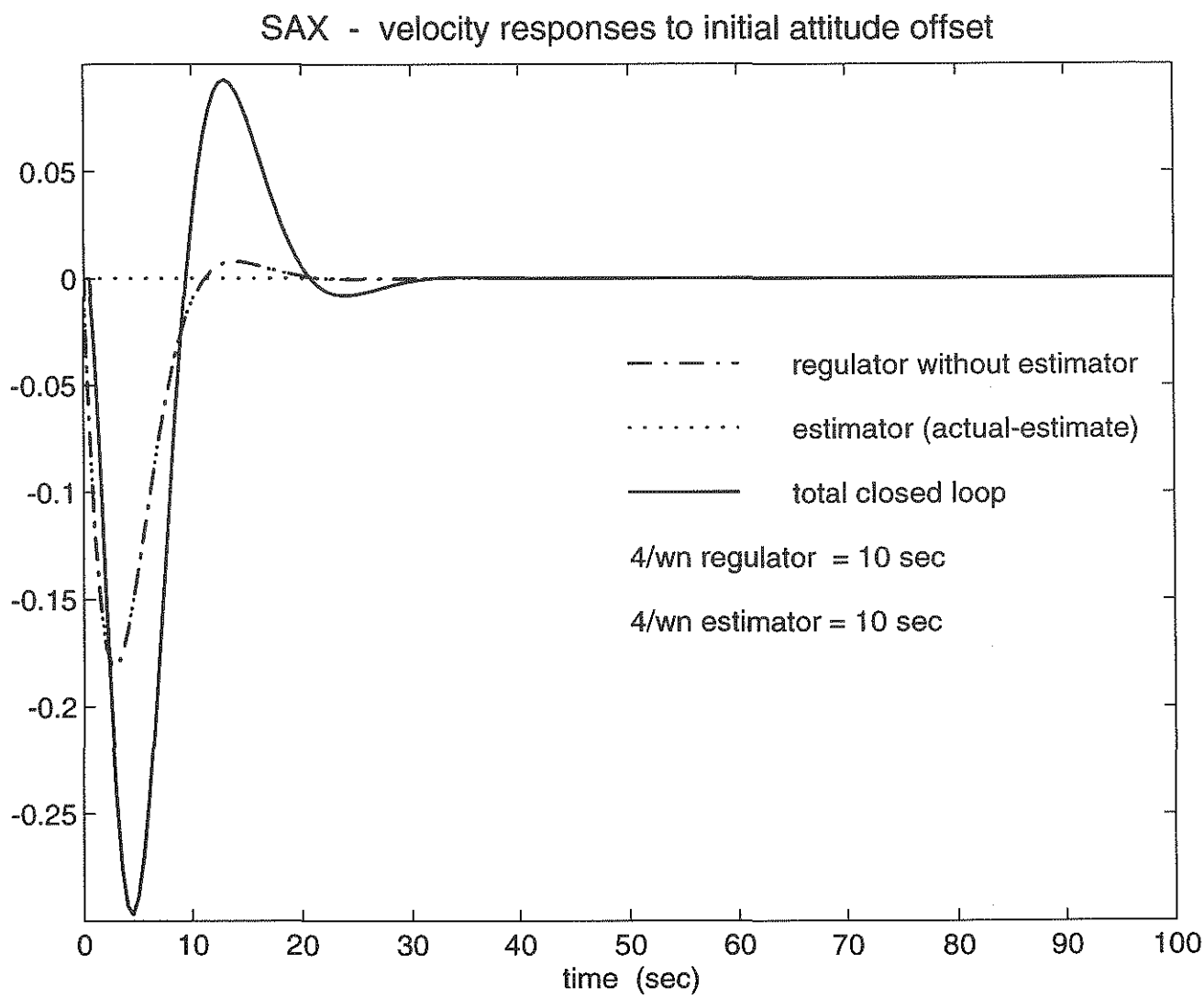

figure 4-2 : Convergence after initial attitude offset.
'fast' regulator
'fast' estimator

(figure 3 of 3)

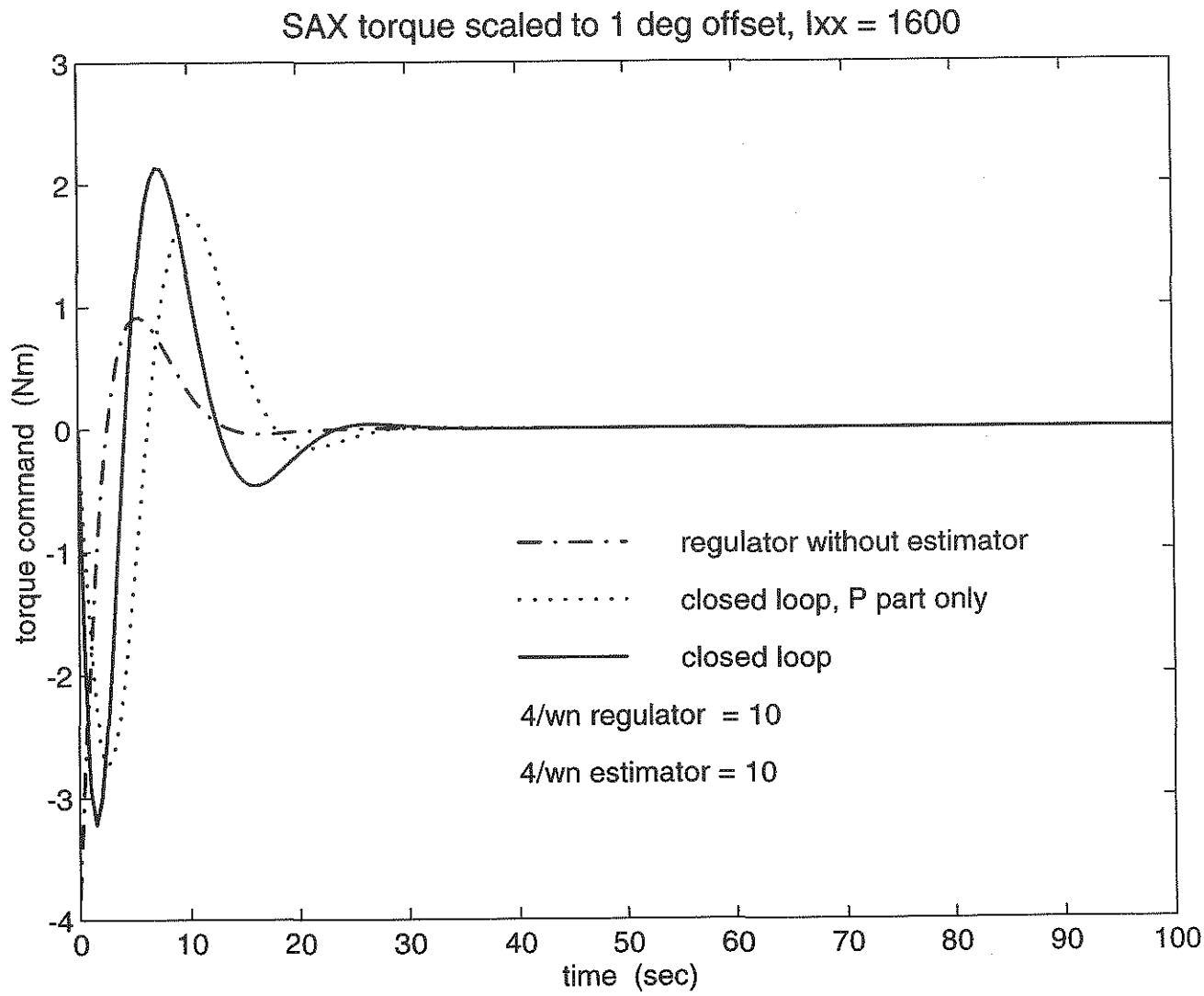

figure 4-3 : Convergence after initial attitude offset.
'fast' regulator
'slow' estimator

(figure 1 of 3)

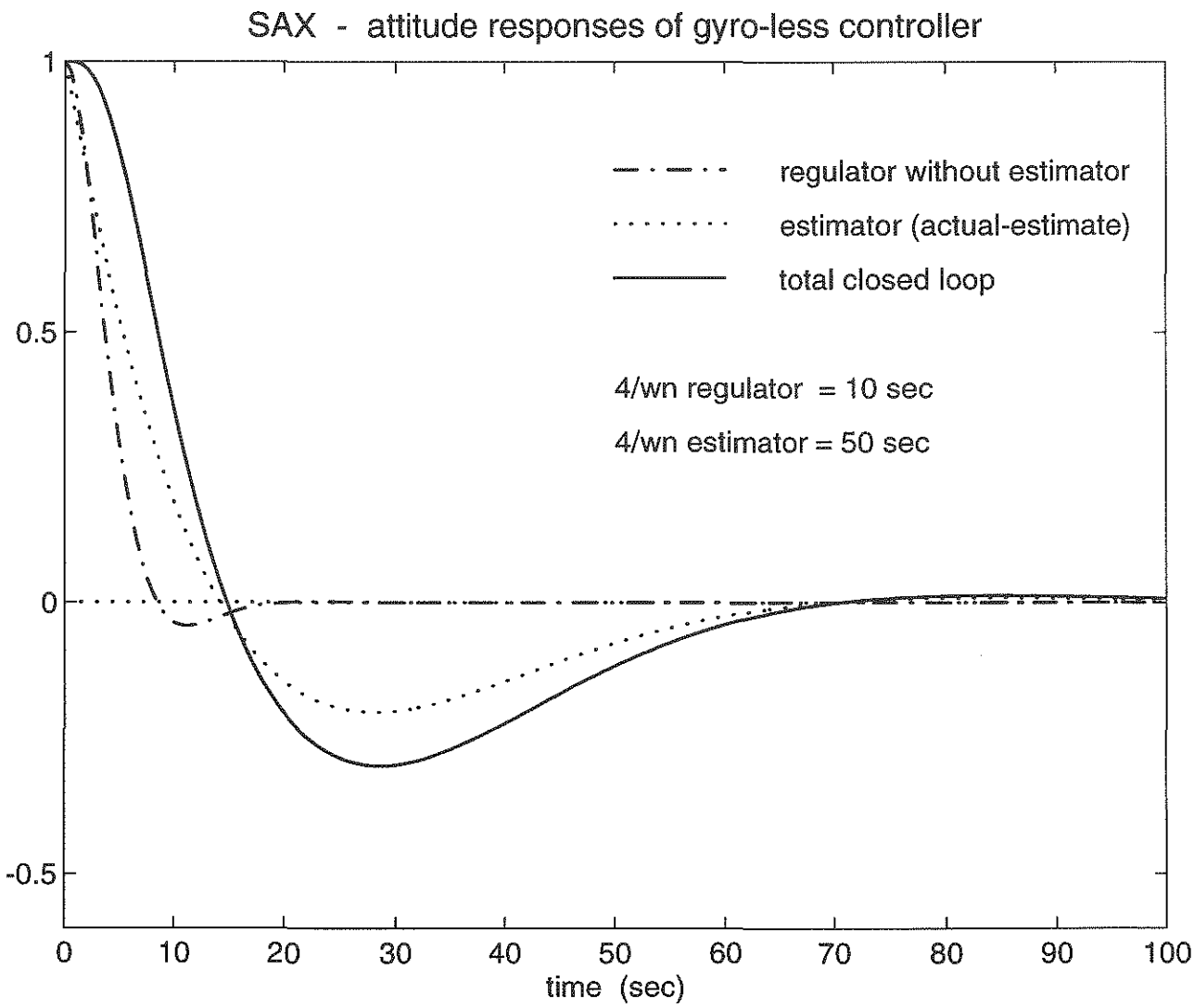

figure 4-3 : Convergence after initial attitude offset.
'fast' regulator
'slow' estimator

(figure 2 of 3)

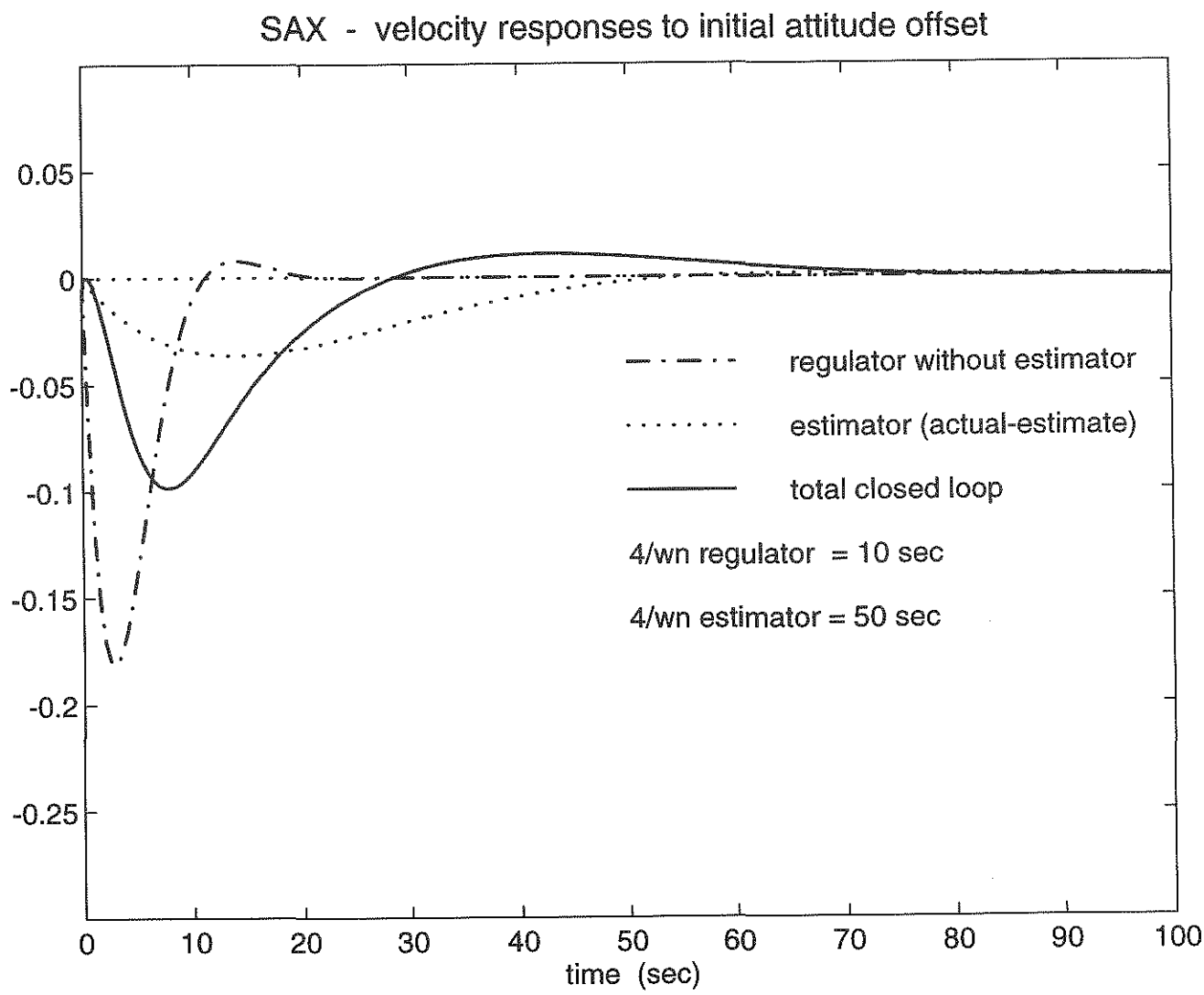

figure 4-3 : Convergence after initial attitude offset.
'fast' regulator
'slow' estimator

(figure 3 of 3)

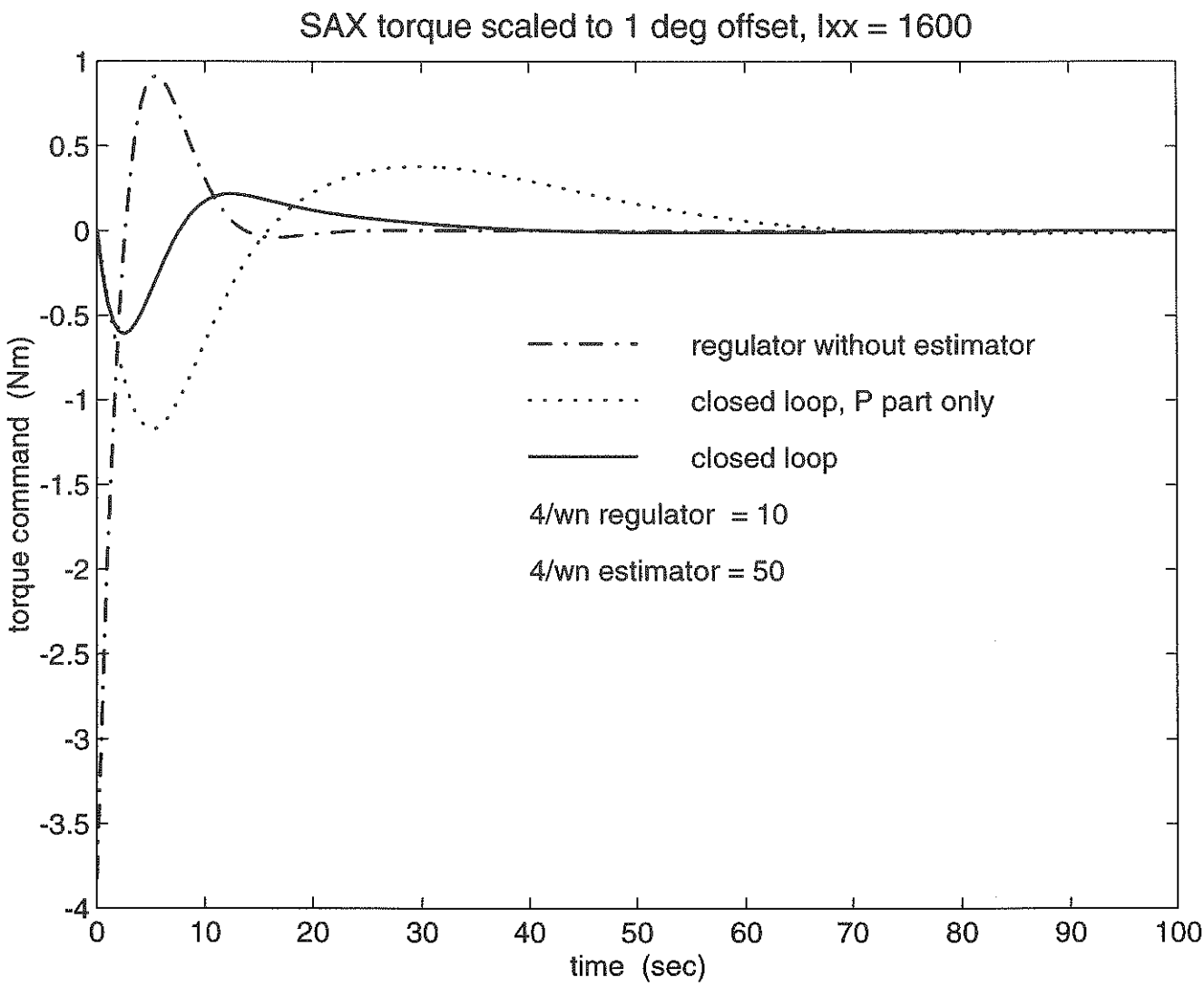

figure 4-4 : Convergence after initial attitude offset.
'slow' regulator
'fast ' estimator

(figure 1 of 3)

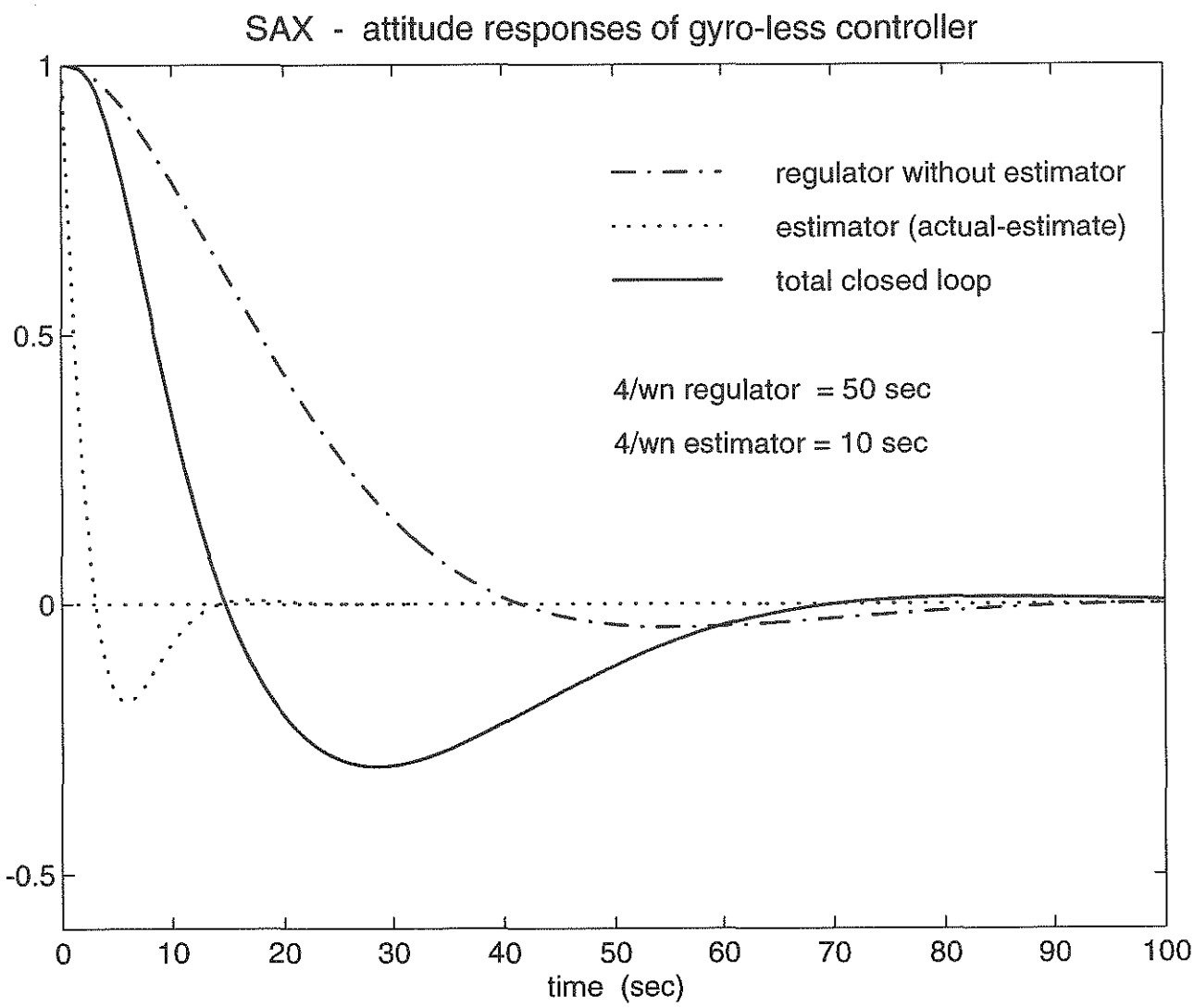

figure 4-4 : Convergence after initial attitude offset.
'slow' regulator
'fast ' estimator

(figure 2 of 3)

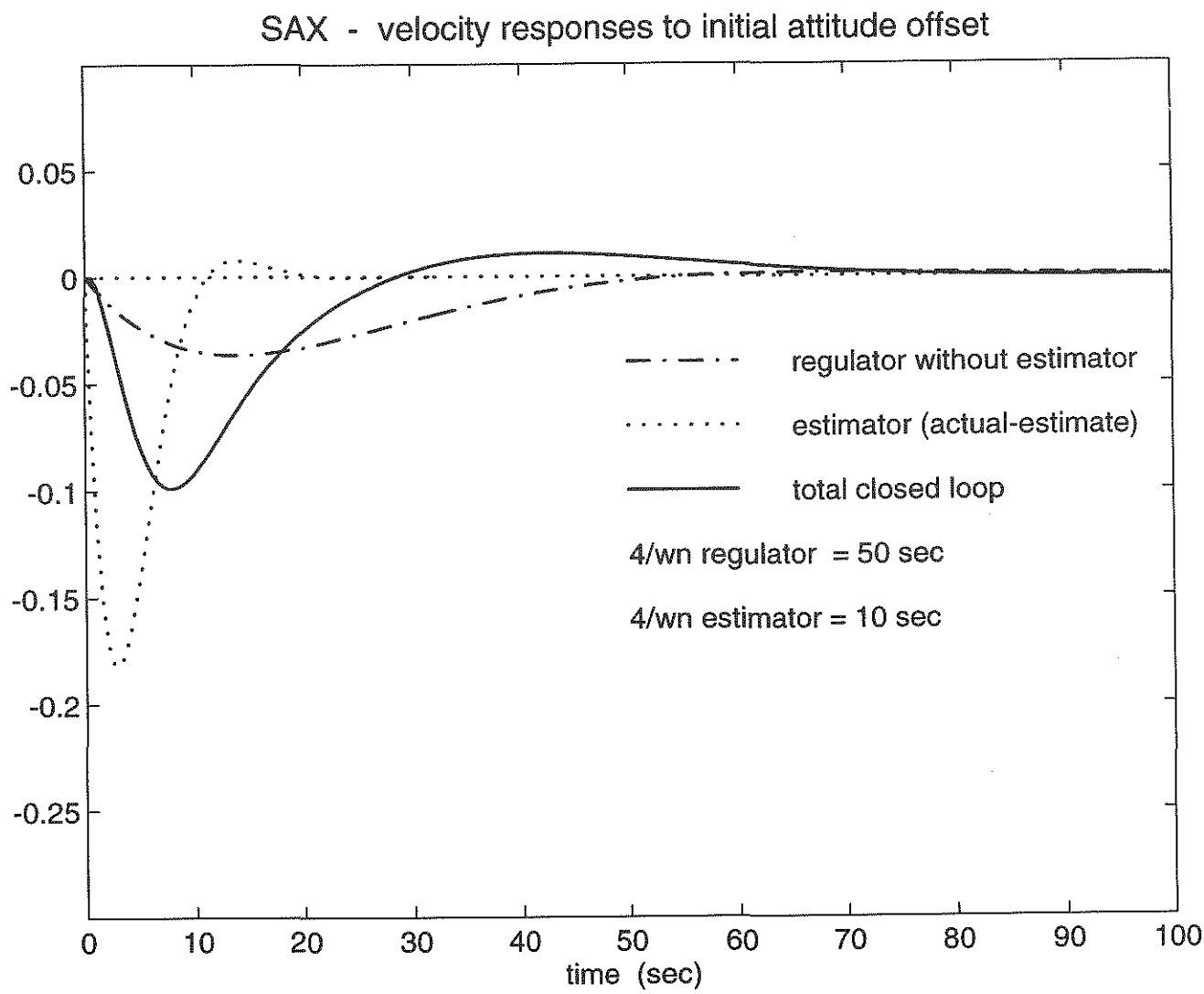

figure 4-4 : Convergence after initial attitude offset.
'slow' regulator
'fast ' estimator

(figure 3 of 3)

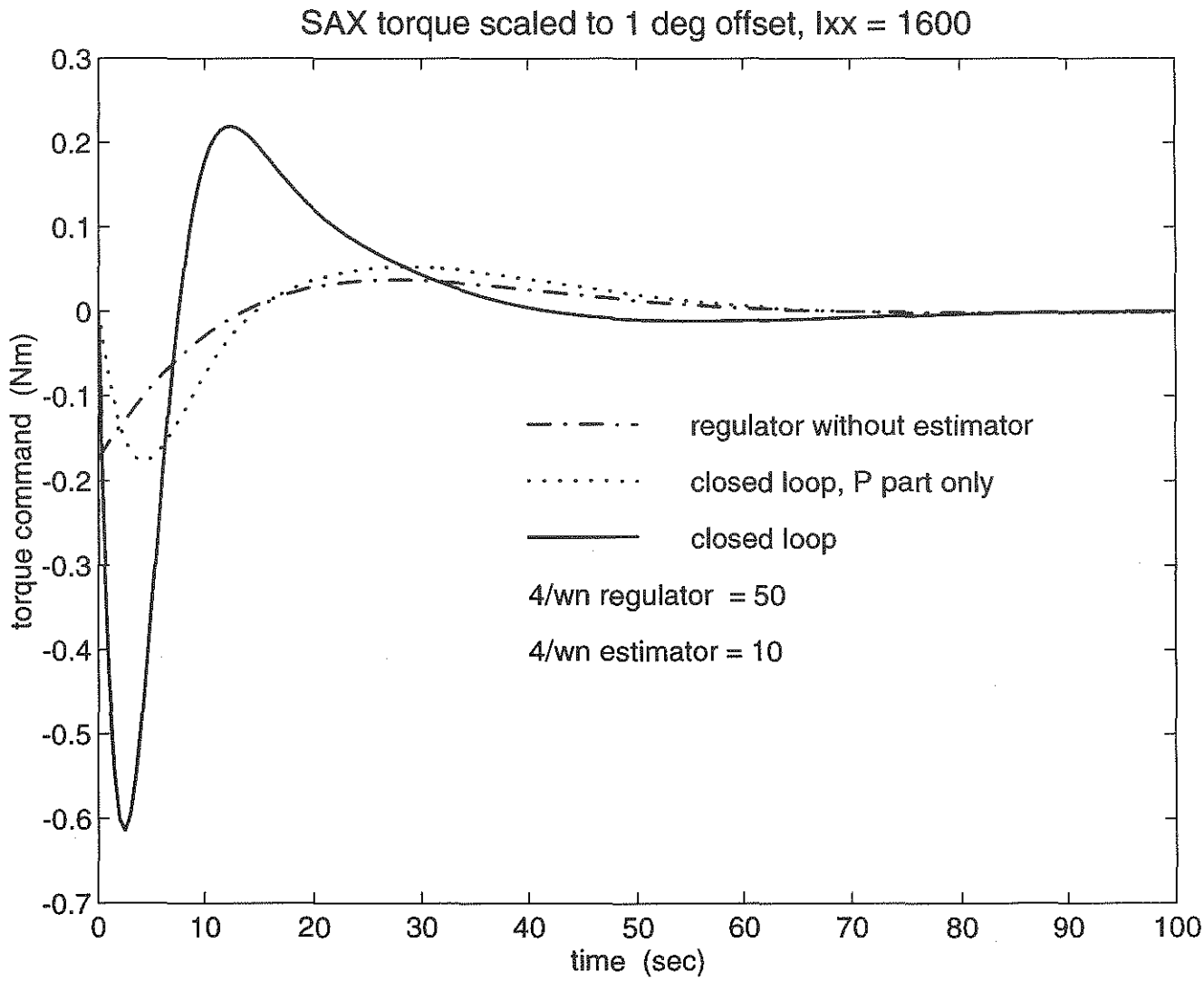

figure 4-5 : Convergence after initial attitude offset.
'slow' regulator
'slow' estimator

(figure 1 of 3)

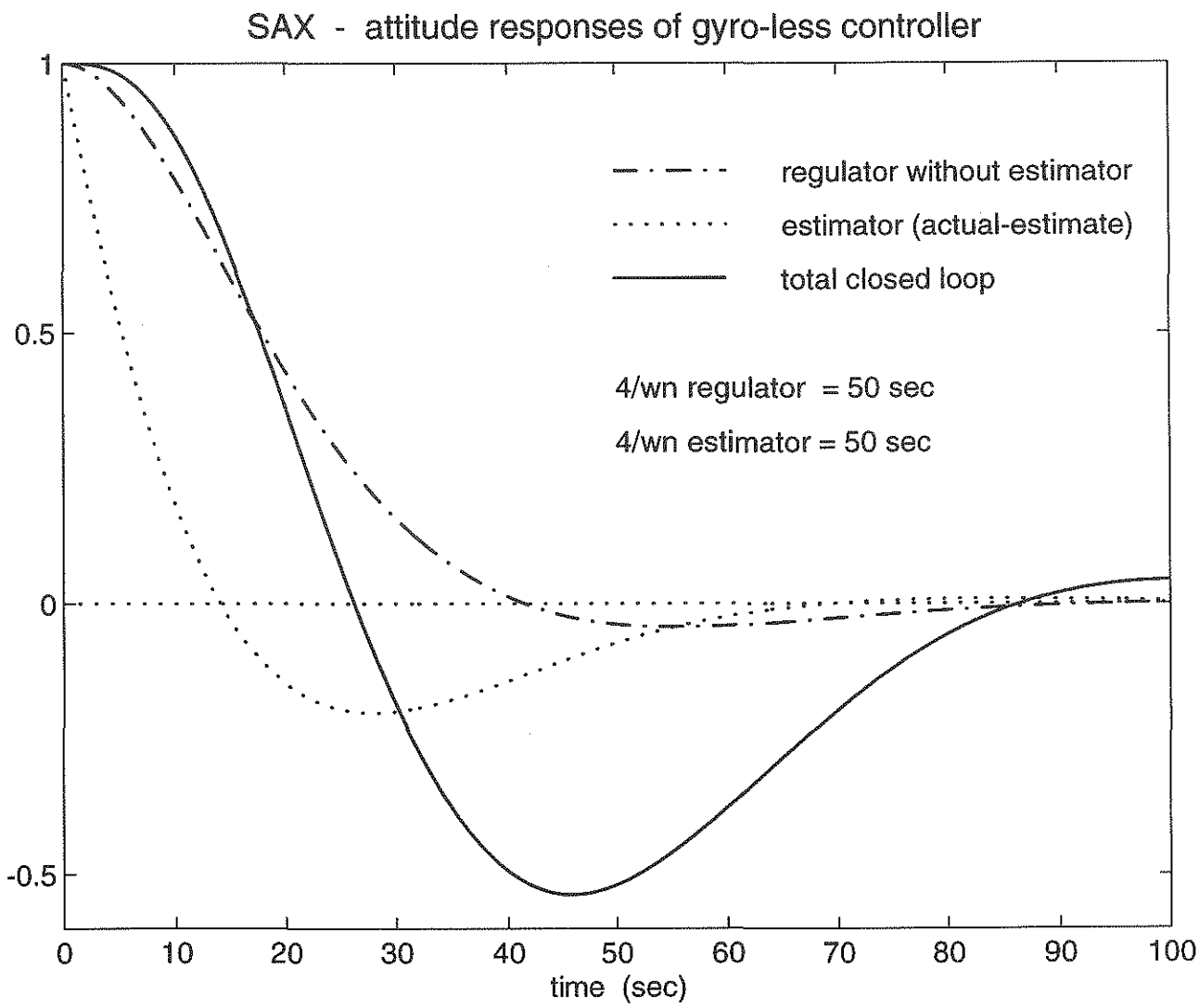

figure 4-5 : Convergence after initial attitude offset.
'slow' regulator
'slow' estimator

(figure 2 of 3)

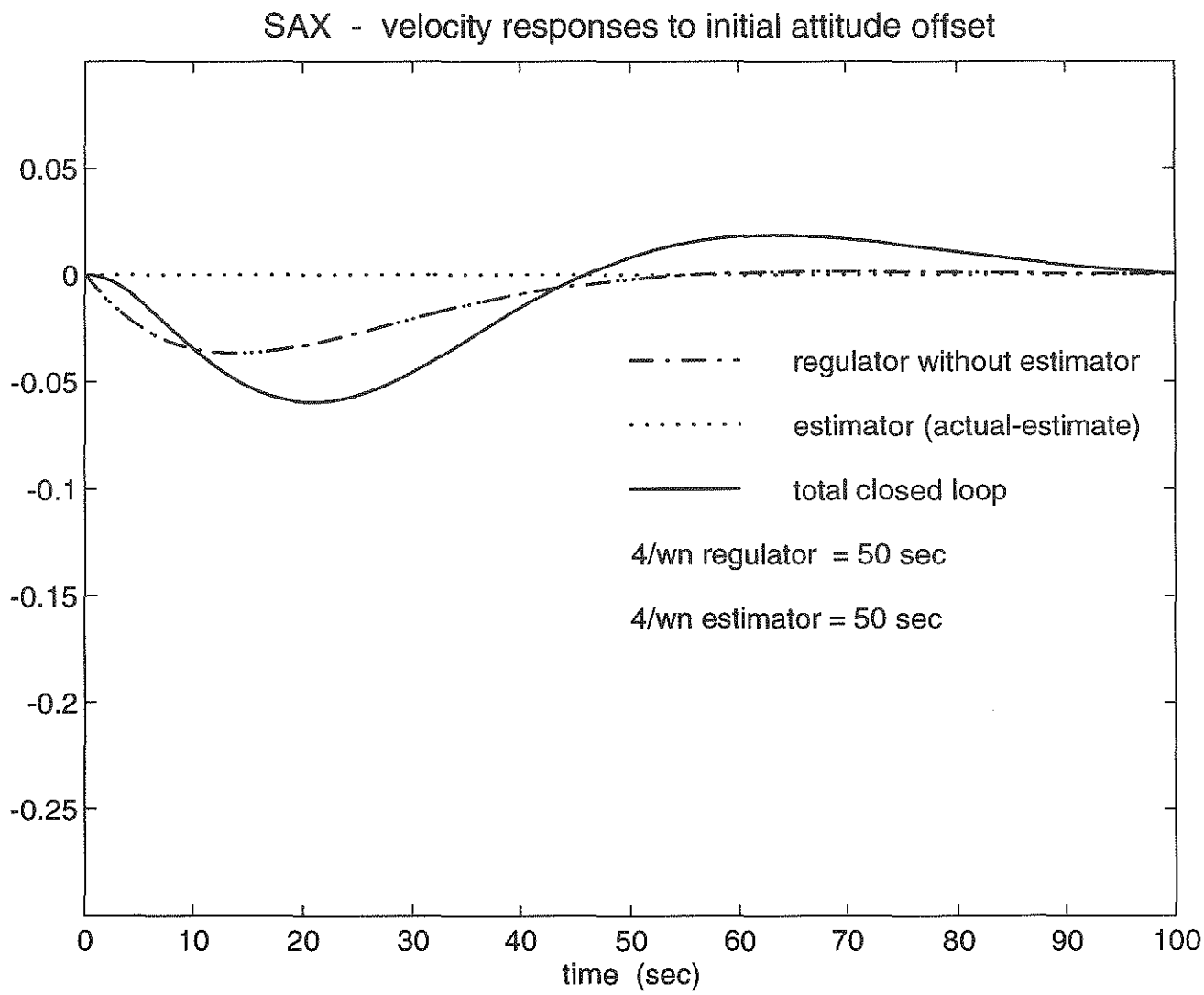

figure 4-5 : Convergence after initial attitude offset.
'slow' regulator
'slow' estimator

(figure 3 of 3)

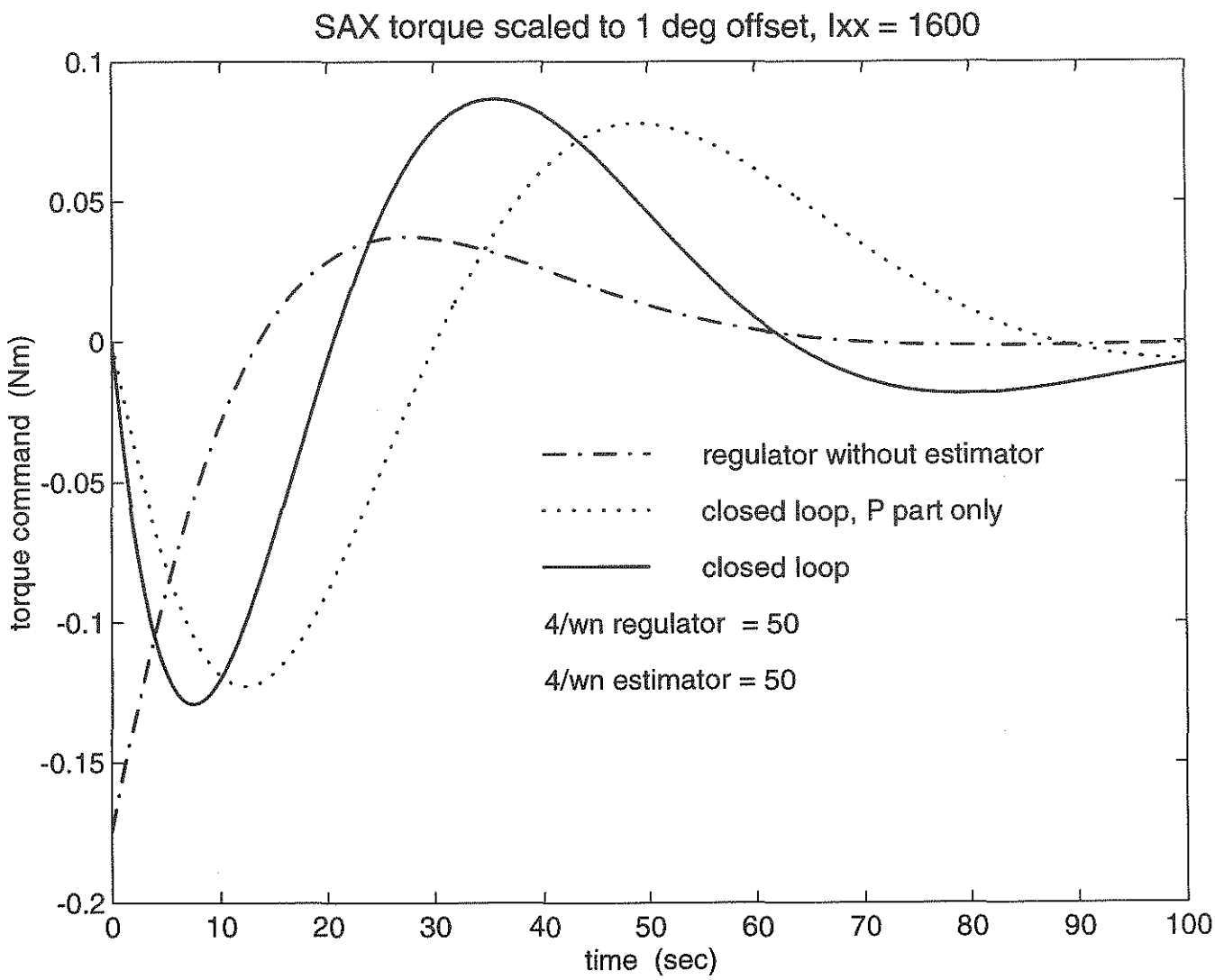

figure 4-6 : Convergence after initial attitude offset. evens slower regulator and estimator

(figure 1 of 3)

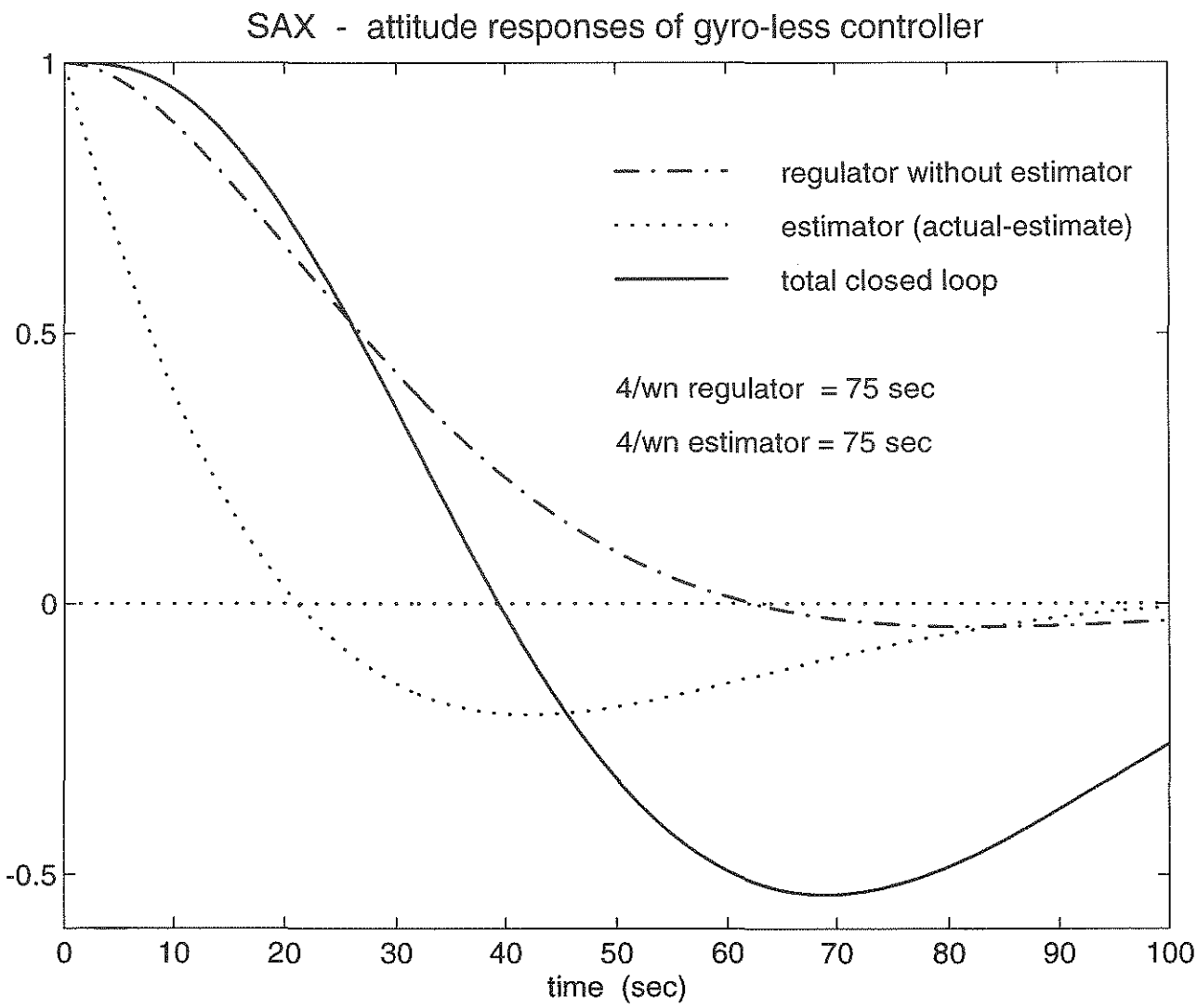

figure 4-6 : Convergence after initial attitude offset. evens slower regulator and estimator

(figure 2 of 3)

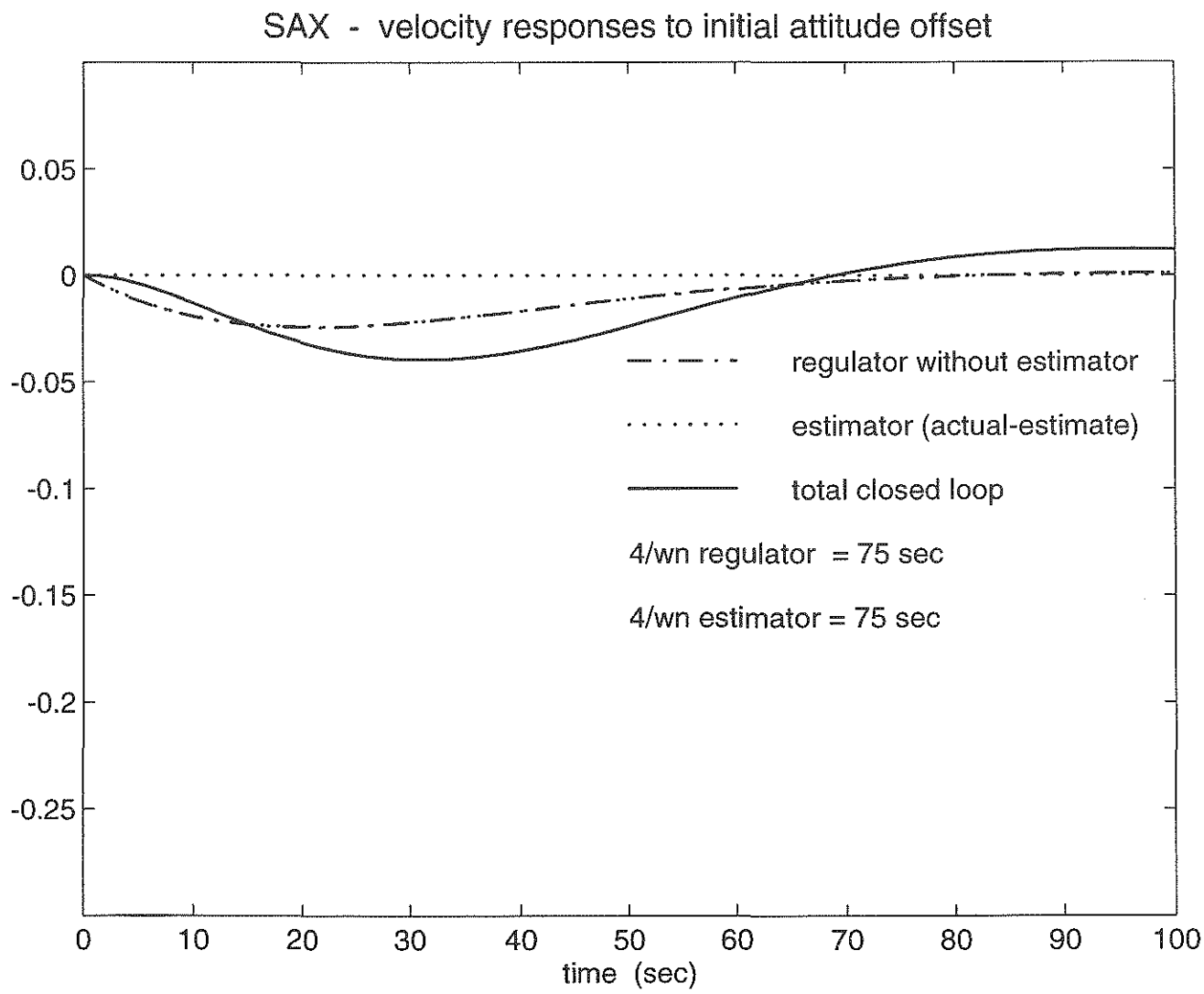

figure 4-6 : Convergence after initial attitude offset. evens slower regulator and estimator

(figure 3 of 3)

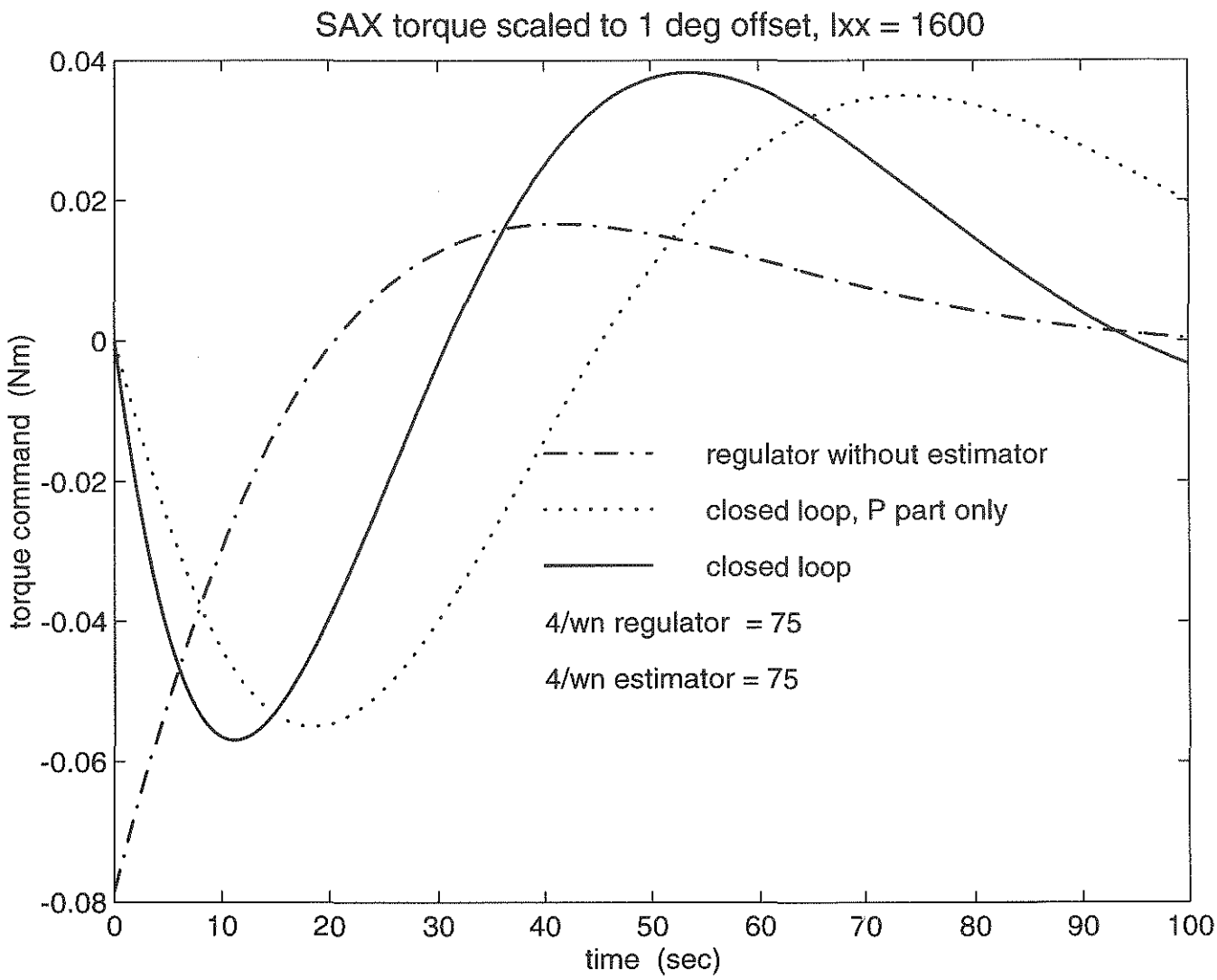

figure 4-7 : Response to a spike in MGM output.
'slow' regulator
'fast' estimator

(figure 1 of 3)

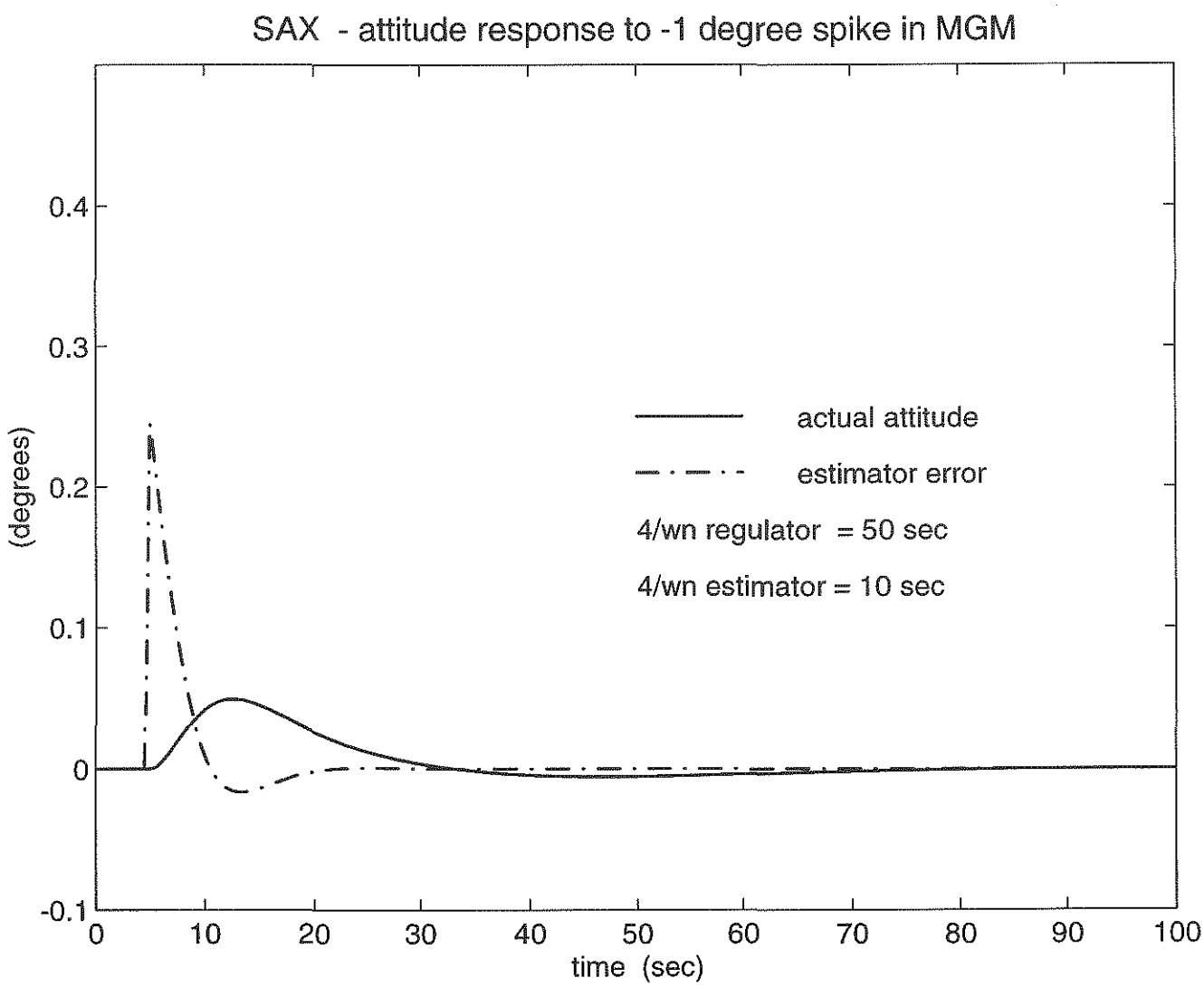

figure 4-7 : Response to a spike in MGM output.
'slow' regulator
'fast' estimator

(figure 2 of 3)

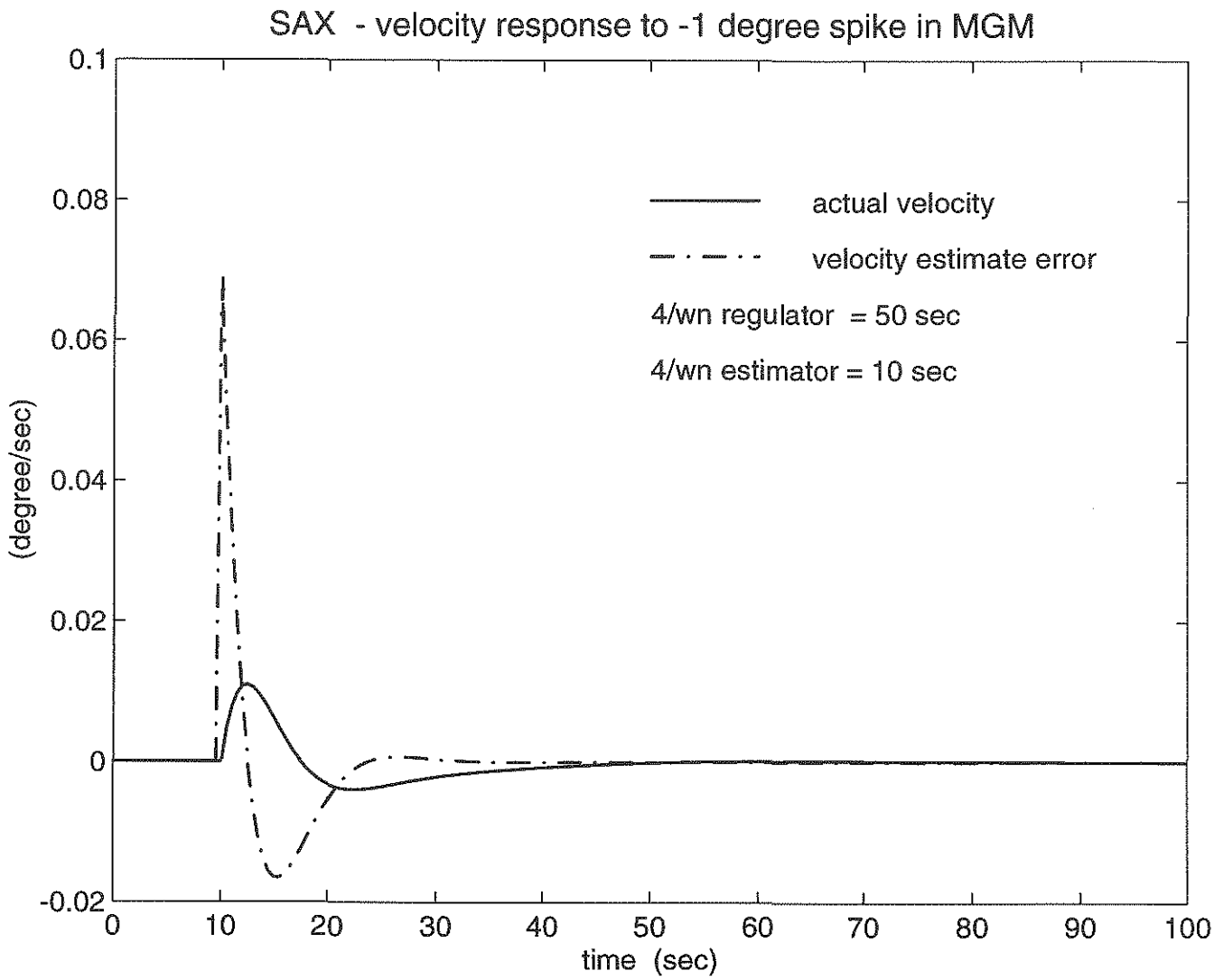

figure 4-7 : Response to a spike in MGM output.
'slow' regulator
'fast' estimator

(figure 3 of 3)

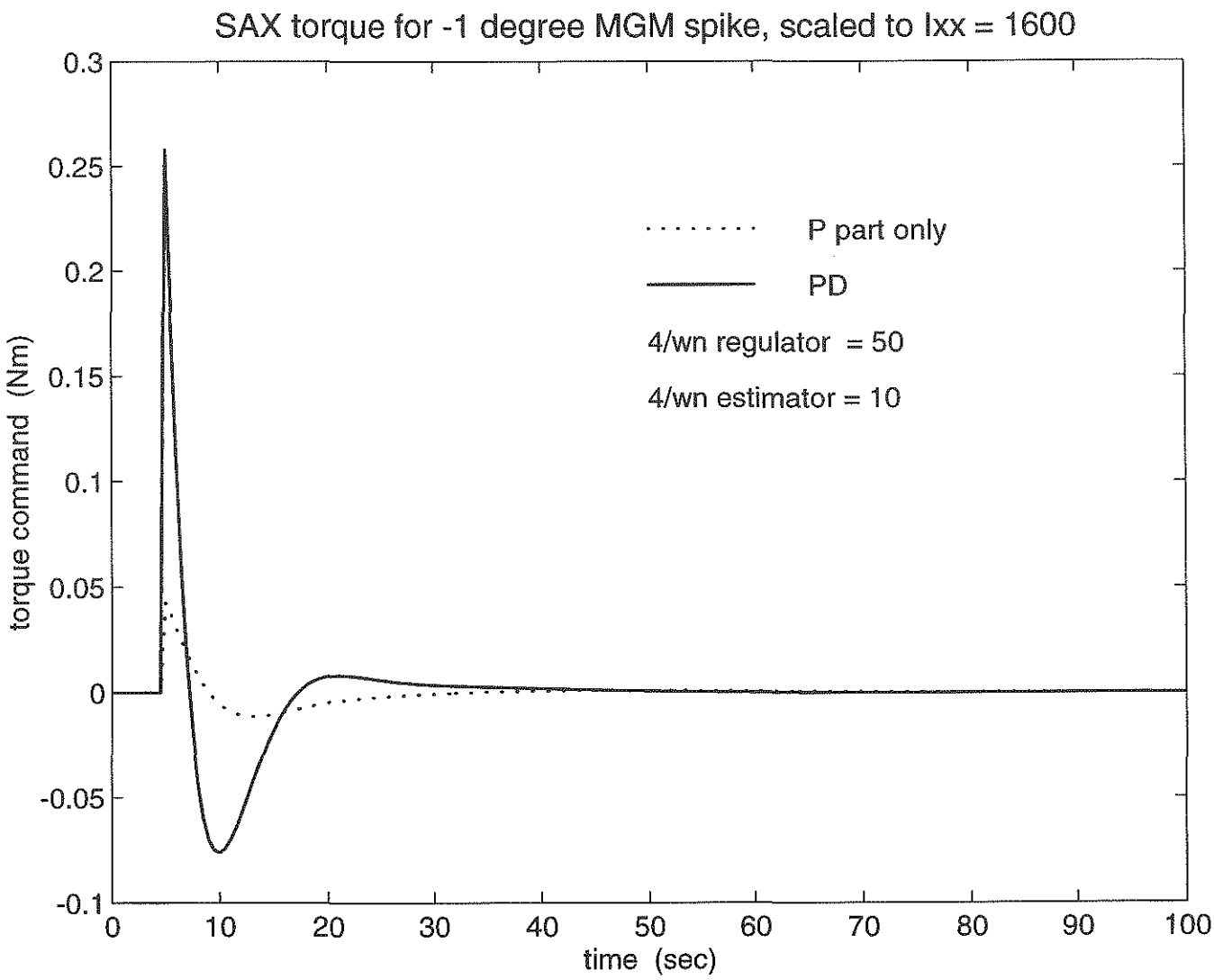

figure 4-8 : Reponse to a spike in MGM output.
'slow' regulator
'slow' estimator

(figure 1 of 3)

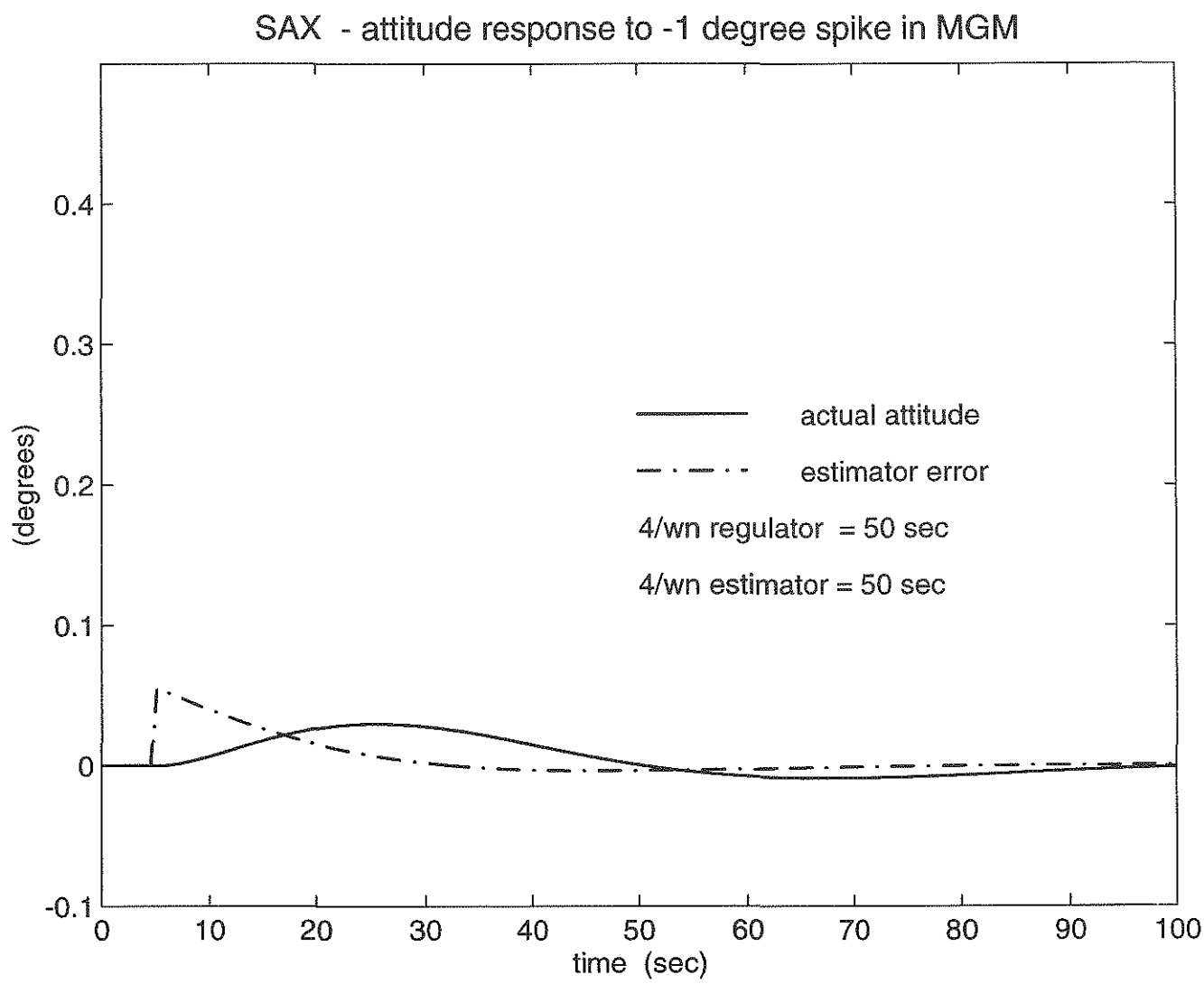

figure 4-8 : Reponse to a spike in MGM output.
'slow' regulator
'slow' estimator

(figure 2 of 3)

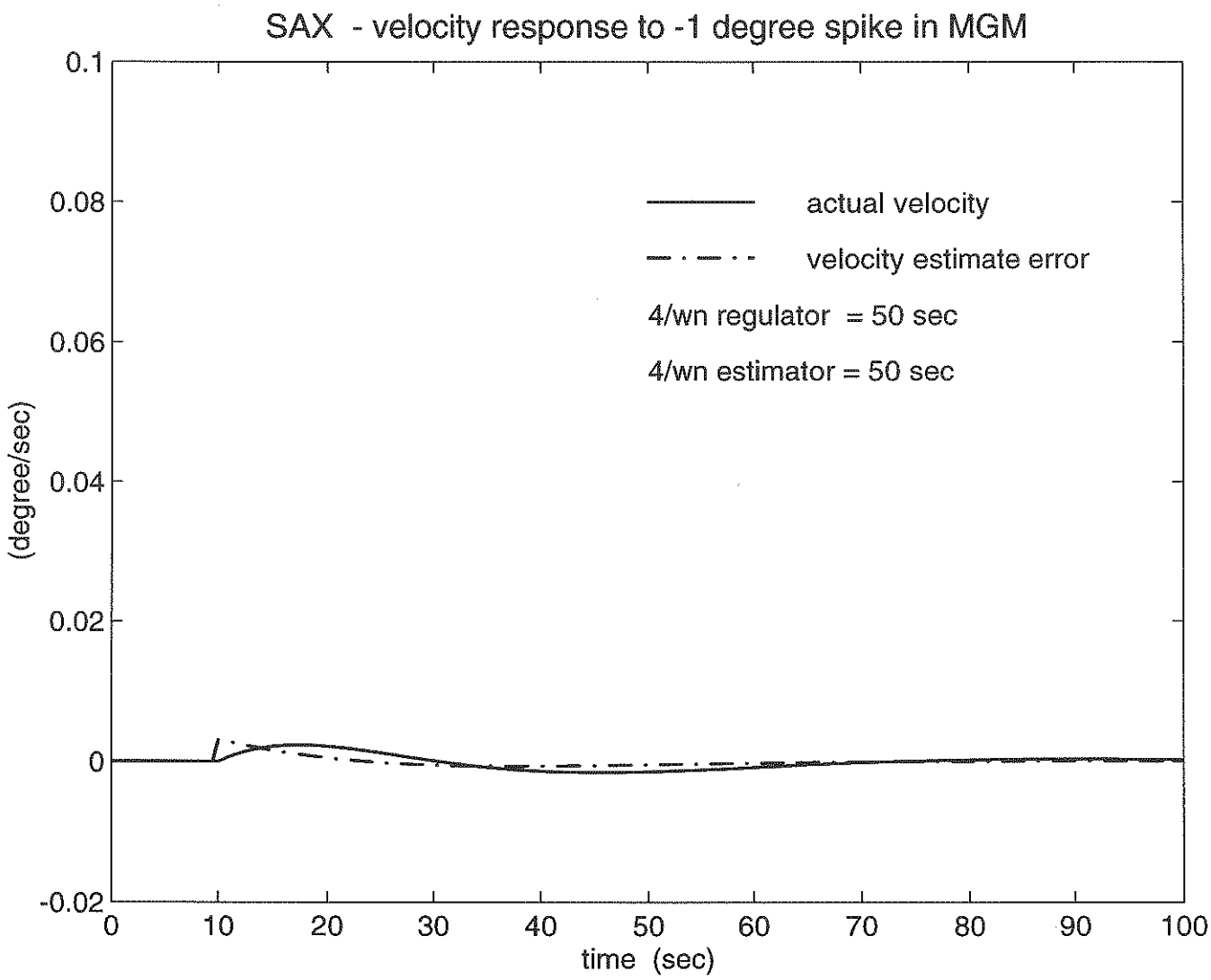

figure 4-8 : Reponse to a spike in MGM output.
'slow' regulator
'slow' estimator

(figure 3 of 3)

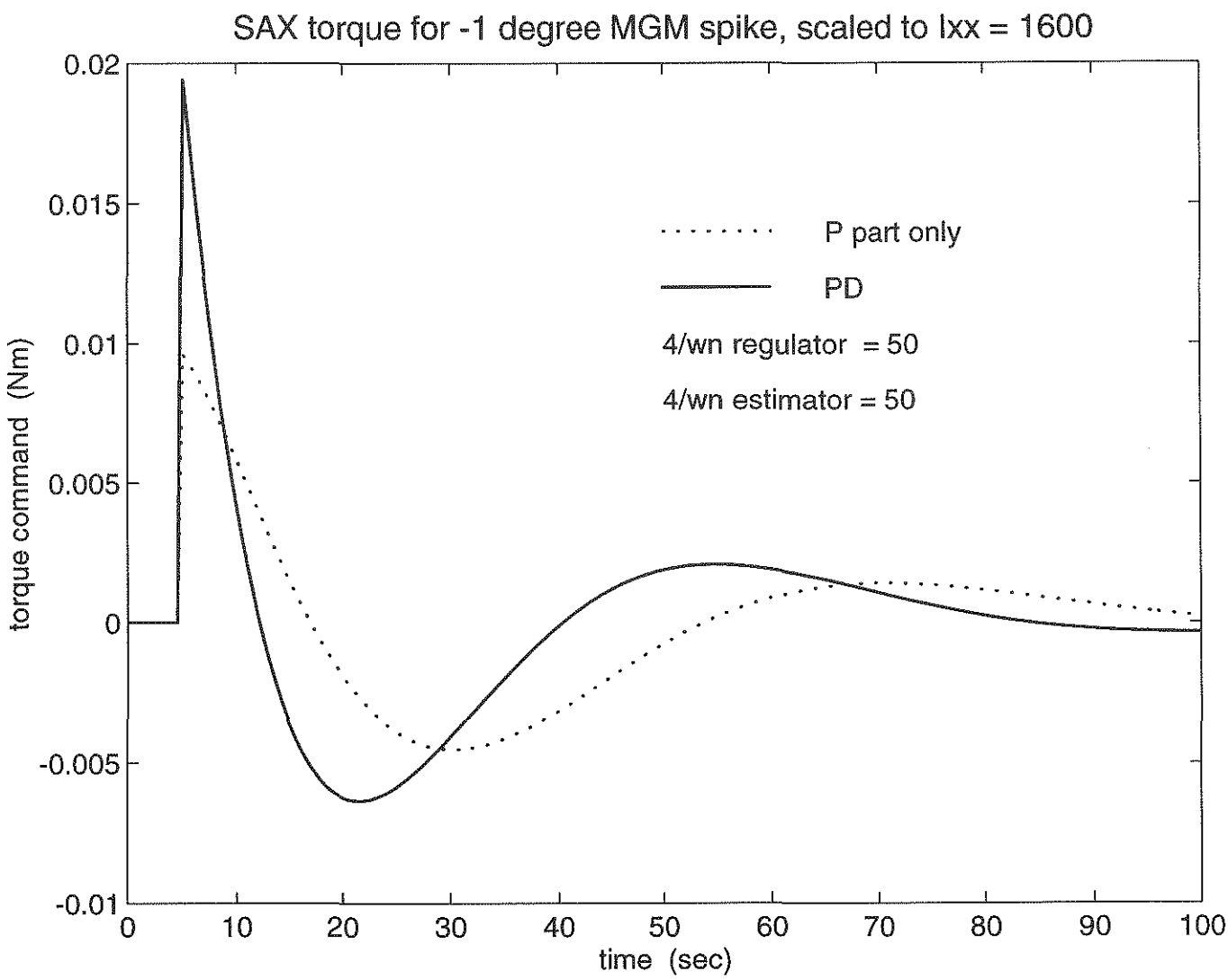

figure 4-9 : Convergence after initial attitude offset.

settings used in Alenia design simulations
(figure 1 of 3)

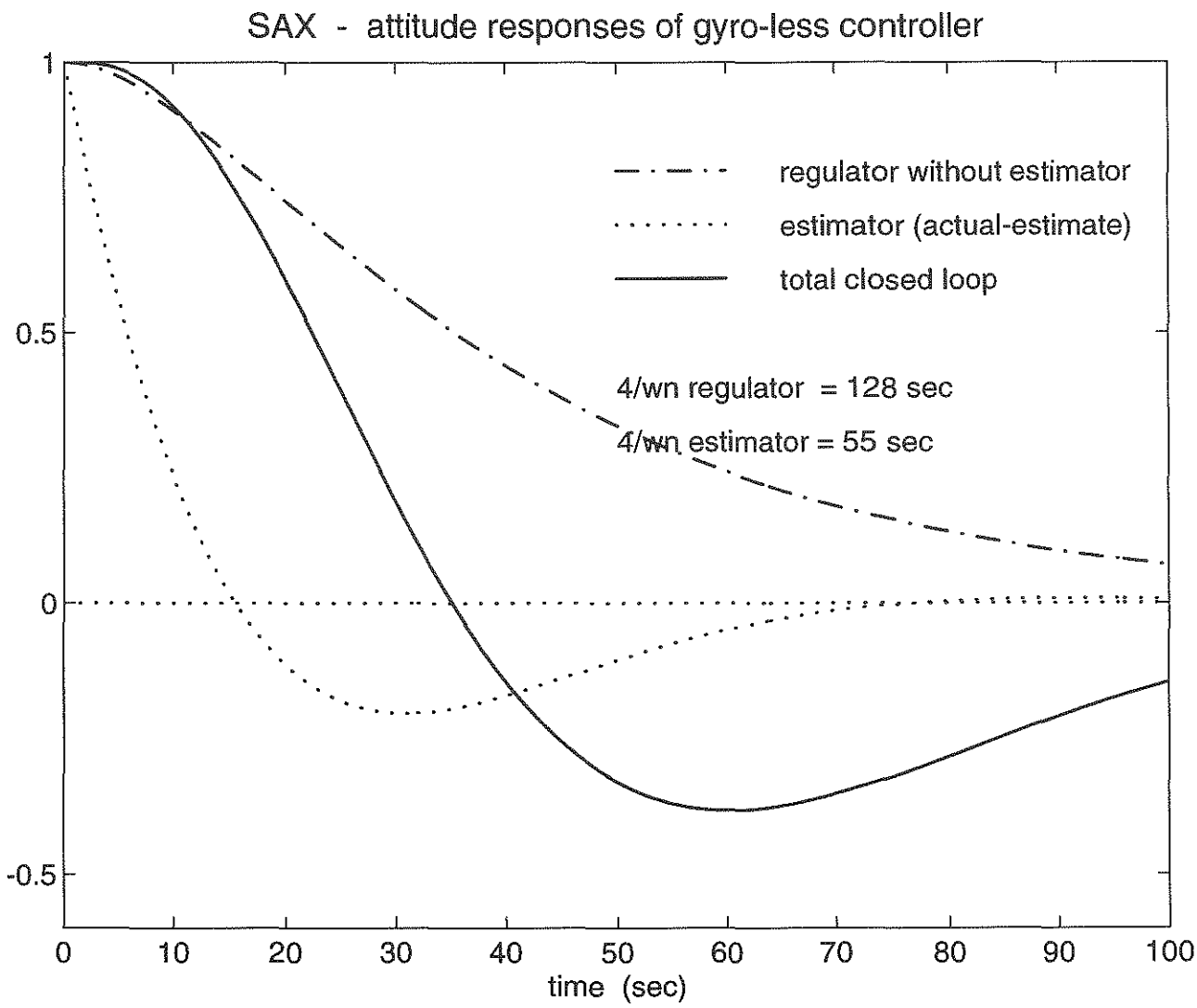

figure 4-9 : Convergence after initial attitude offset.

settings used in Alenia design simulations
(figure 2 of 3)

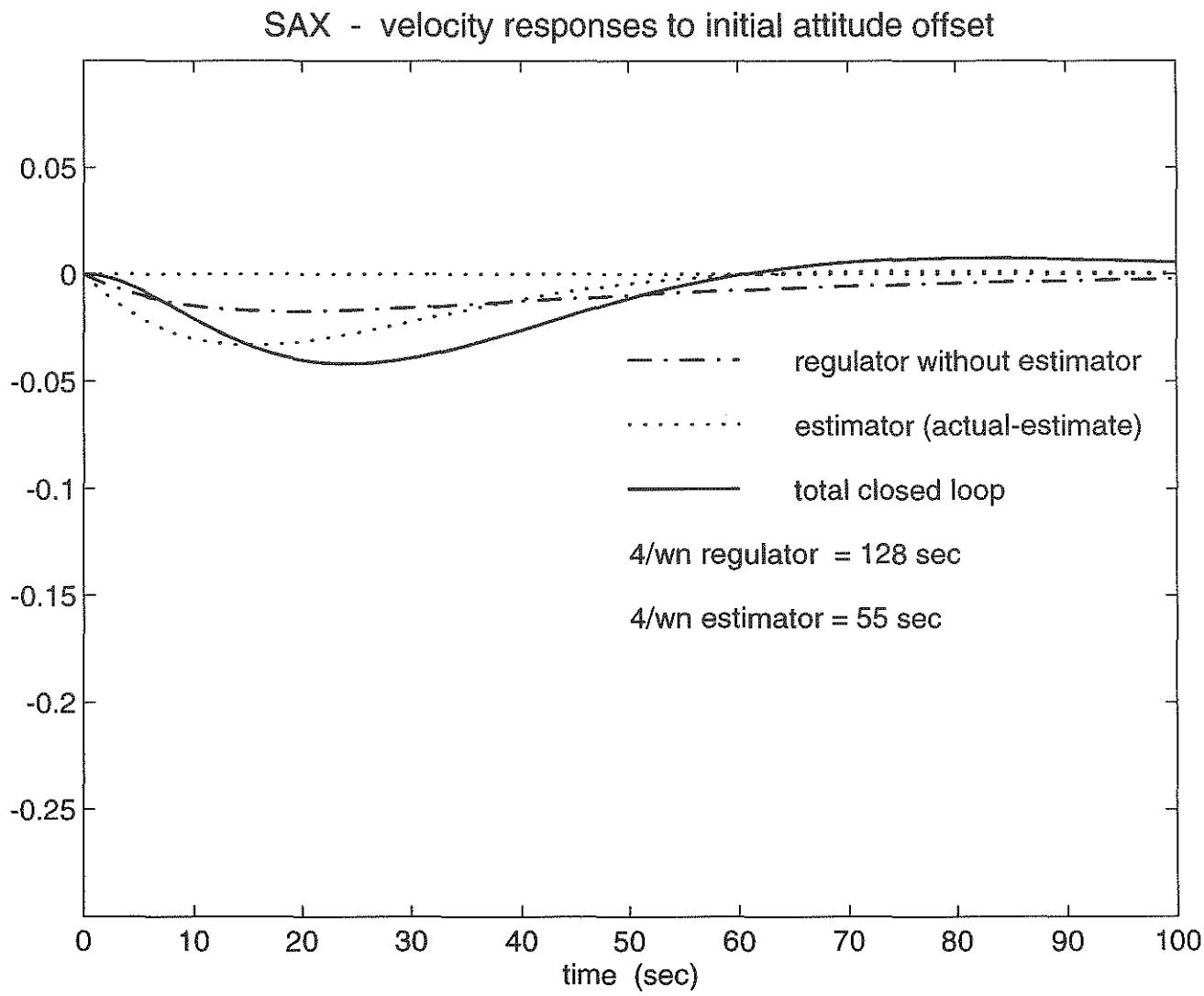

figure 4-9 : Convergence after initial attitude offset.

settings used in Alenia design simulations
(figure 3 of 3)

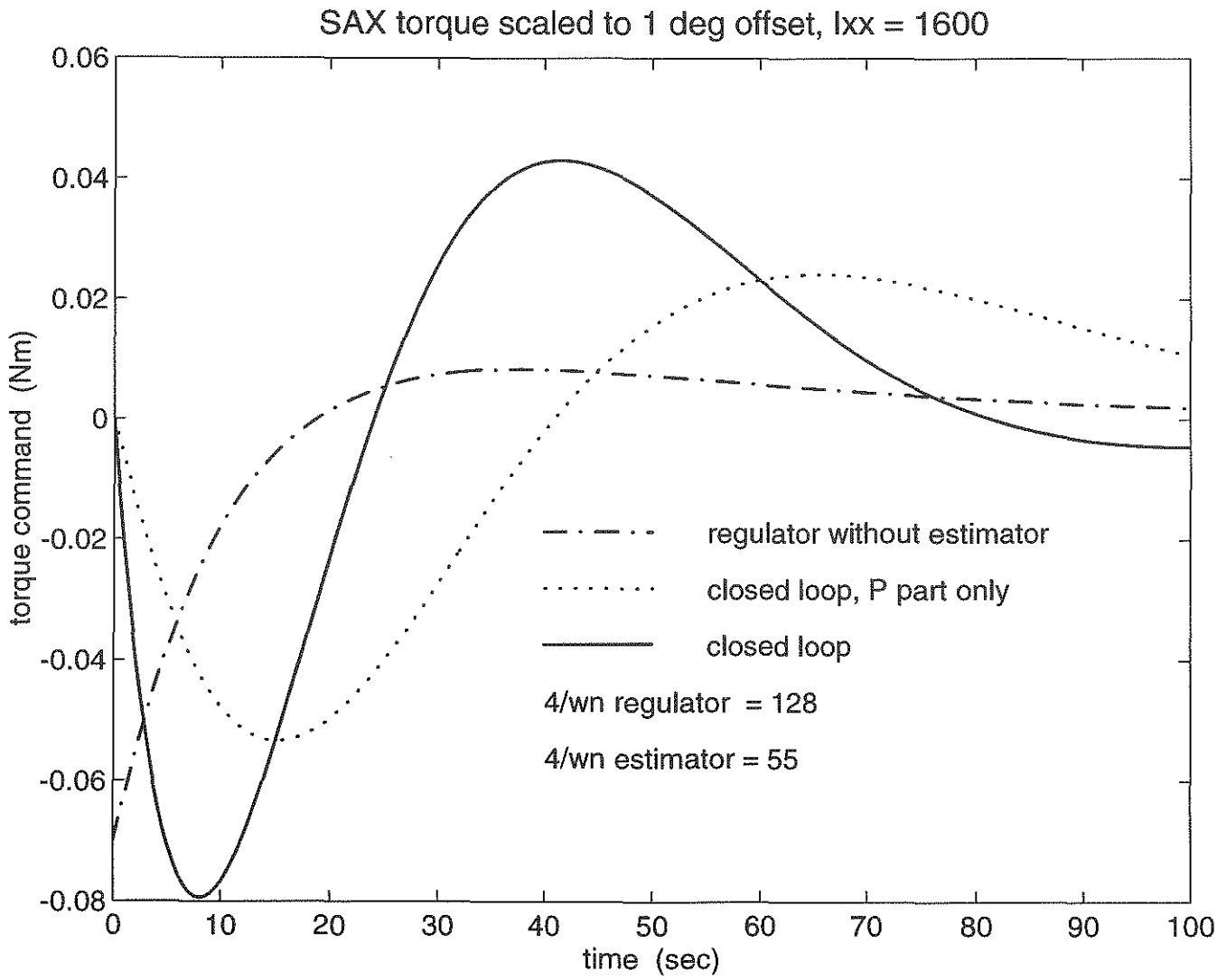

A Appendix A - RWS thermal model

The main problems which can be expected from unsatisfactory closed loop control behaviour are :

- excitation of the flexible modes of the solar panels.
- mechanical and thermal stress on the reaction wheel system.

The flexibility of the solar panels is already modelled in full-scale SAX simulations; however, a thermal model of the reaction wheels is currently not included. A simple and effective model of the Teldix reaction wheels has been used in the design and verification simulations of the ISO satellite. The following pages give enough relevant documentation to copy this model. If an electrical model of the reaction wheels, in particular a model of the motor coil current, is included in the SAX simulations, then adding this thermal model should be quite simple. It is noted that in ISO simulations it has become obvious that the middle node (motor casing) can be omitted if desired, since it never varies more than a few degrees in temperature from the boundary node (satellite body). This leaves only a single node which varies in temperature, viz. the motor coils. These are in fact the critical item in the thermal design of the reaction wheels.

No hard and fast maximum allowable coil temperature has been defined in ISO, but it has been accepted that if the temperature of the coils exceeds 95 degrees centigrade for any length of time, the wheels will eventually fail due to degradation of the coil isolation. The ISO satellite body has been assumed to have a worst case operational temperature of 43 degrees centigrade in this context.

A Appendix A - RWS thermal model

The main problems which can be expected from unsatisfactory closed loop control behaviour are :

- excitation of the flexible modes of the solar panels.
- mechanical and thermal stress on the reaction wheel system.

The flexibility of the solar panels is already modelled in full-scale SAX simulations; however, a thermal model of the reaction wheels is currently not included. A simple and effective model of the Teldix reaction wheels has been used in the design and verification simulations of the ISO satellite. The following pages give enough relevant documentation to copy this model. If an electrical model of the reaction wheels, in particular a model of the motor coil current, is included in the SAX simulations, then adding this thermal model should be quite simple. It is noted that in ISO simulations it has become obvious that the middle node (motor casing) can be omitted if desired, since it never varies more than a few degrees in temperature from the boundary node (satellite body). This leaves only a single node which varies in temperature, viz. the motor coils. These are in fact the critical item in the thermal design of the reaction wheels.

No hard and fast maximum allowable coil temperature has been defined in ISO, but it has been accepted that if the temperature of the coils exceeds 95 centigrade for any length of time, the wheels will eventually fail due to degradation of the coil isolation. The ISO satellite body has been assumed to have a worst case operational temperature of 43 degrees centigrade in this context.

for: Freyer Chiavichy
at Alenia Torino

ISO → SAX

7.2.3.4 RWS thermal model

The thermal model of the RWL has been simplified to a three-node model. The model uses the power dissipation figures of the power consumption model as input, and gives the temperature of the nodes as output.

Figure 7.2-2 on the next page shows the schematic of the model. The nodes are:

node 1 : motor windings
node 2 : box walls
node 3 : baseplate (reference temperature)

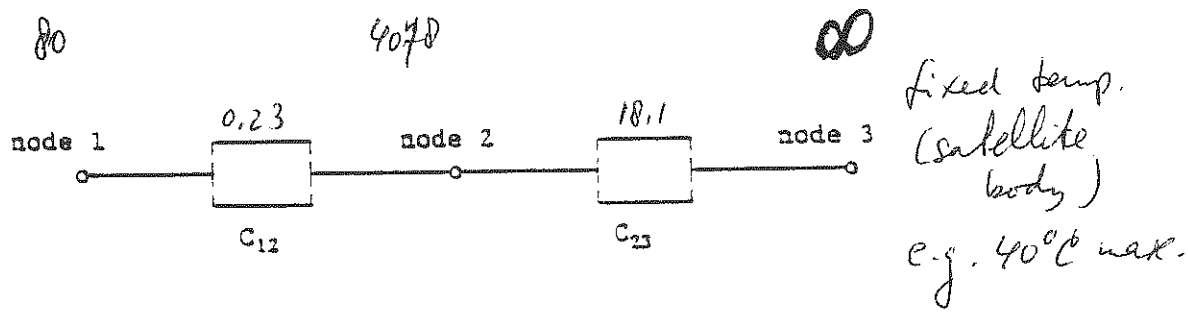

Figure 7.2-2 Three node thermal model of RWL

Heat capacity and conductances

The heat capacities of nodes 1, 2 are model parameters: G1 and G2. The conductances between the nodes, C_{12} and C_{23} are also model parameters.

Baseplate reference temperature

Node 3 has an infinite heat capacity or, in other words, a constant temperature. This temperature, $T_{baseplate}$, is a model parameter.

Calculate heat influxes

The heat influx in node 1 of each motor (the motor windings) is the electrical heat plus the motor loss torque. This torque T_{lm} is a part of the total loss torque T_L. Multiplied with W it defines the amount of mechanical heat produced near the motor windings.

The heat influx for node 2 (the box walls) is the total power dissipated minus the power dissipated in node 1 (the motor windings).

$$P_1 = I_m^2 \quad Z_m + T_{lm} \quad |W|$$

$$P_2 = PRWLDIS - P_1$$

Calculate new temperatures

The temperature of node 1 (motor windings) and node 2 (box walls) for each wheel is adapted each integration time step dt by numerical integration of the heat flow equation:

$$T_{coil} = T_{coil} + dt \cdot (G_{12} \cdot (T_{box} - T_{coil}) + P1) / C1$$

$$T_{box} = T_{box} + dt \cdot (G_{12} \cdot (T_{coil} - T_{box}) + G_{23} \cdot (T_{base} - T_{box}) + P2) / C2$$

Thermal model parameters

The following parameters are used in the thermal modelling of the reaction wheels:

symbol	value	unit	description	SLR
G_{12}	0.23	W/K	motor coil - box wall heat conductance	190
G_{23}	18.1	W/K	box wall - base plate heat conductance	190
C_1	80.0	J/K	motor coil heat capacity	190
C_2	4078.0	J/K	box wall heat capacity	190
T_{lm}	$\frac{1}{3}$ * 3.0E-3	Nm	motor loss torque	190

The following parameters are fixed in the software:

symbol	value	unit	description	SLR	
T_{coil}	43°	°C	motor coil initial temperature	190	3A
T_{box}	43°	°C	box wall initial temperature	190	3A
T_{base}	43°	°C	baseplate initial temperature	190	3A

Tacho resolution

The number of tacho tick marks on the wheel circumference is: 3B

parameter	value	SLR
NC	24	80

The tacho counts tick marks during the first 490 ms of each 500 ms control cycle only. 3B

Note $G_{23} \gg G_{12}$. Node 2 has large capacity and good coupling to spacecraft, and it hardly follows the changes in temperature of node 1 (the motor coil). Node 2 can be left out without problem.

SLR (standard list of references)

113	ISO-1421-A-8000, issue D, STR Interface drawing	
172	ISO-TE-RP-6567, issue 3 Design Report RWS	
173	ISO-GO-RP-3518, issue 2 Design Analysis STR	
173a	fax: ISO/90-678, 12 Mar 1990 Note: data will be compiled in: ISO-GO-RP-3518, issue 3 (TBW !) Design Analysis STR	3B
173b	ISO/465, 14 Sep 1989, OG fax 'AI 816-05'	
173d	RMR-GO-8001, issue 2, Note: data will be compiled in: ISO-GO-RP-3518, issue 3 (TBW !) Design Analysis STR	5A
175	ISO-GO-RE-7056, issue 3A Design Analysis Report ELS	5A
175a	fax: ISO-1686, 25 Feb 1992 Note: data will be compiled in: ISO-GO-RE-7056, issue 4 (TBW !) Design Analysis Report ELS	5A
177	ISO-GO-RP-6017, issue 3A, Design Analysis Report QSS	
189	ISO-TE-RP-6520, issue 3.2, Worst Case Analysis RWS	
190	ISO-TE-RP-6542, issue 5, Thermal Analysis RWS	
203	ISO-FO-MEM-641, 5 Jan 1989 'GYR model'	
204	TPD-ISO-SAS-TN2, issue 1 Worst Case Analysis SAS	
205	ISO-FO-TN-0092, issue 1 ELS modelling	
317	ISO-FO-TN-6068, issue 3, QSS Performance Summary Report (QM)	
328	fax FER-ISO-773, Ferranti Departmental Memo on gyro quantization dd. 921123 and 921218.	5B
...	Ferranti waiver on gyro noise, NEA = 0.4 arcs (TBW)	5B